UNIVERSITÀ DEGLI STUDI DI PADOVA

SCUOLA DI SCIENZE

DIPARTIMENTO DI GEOSCIENZE

Direttore Prof.ssa Cristina Stefani

TESI DI LAUREA MAGISTRALE

IN

GEOLOGIA E GEOLOGIA TECNICA

COLOR VARIEGATION AND INNER STRATIFIED STRUCTURE OF COMET 67P/CHURYUMOV-GERASIMENKO

Relatore: *Prof. Matteo Massironi*

Correlatori: *Dott.ssa Sabrina Ferrari*

Dott.ssa Fiorangela La Forgia

Laureando: *Gloria Tognon*

ANNO ACCADEMICO 2016/2017

Contents

Riassunto

La missione spaziale internazionale Rosetta fu approvata nel 1993 dall'Agenzia Spaziale Europea (ESA), all'interno del programma Horizon 2000 per l'esplorazione dei corpi minori del Sistema Solare, e lanciata il 2 Marzo 2004. Lo spacecraft era composto dall'orbiter Rosetta e dal lander Philae, quest'ultimo progettato per ancorarsi al nucleo della cometa, raccogliere immagini ed effettuare analisi della superficie. La missione si è conclusa nel Settembre del 2016 con l'atterraggio controllato dello spacecraft sulla cometa.

Gli strumenti a bordo del satellite sono stati scelti per effettuare un ampi range di analisi, fra cui analisi d'immagine, spettroscopia e spettrofotometria. In particolare, le immagini usate per questo lavoro sono state acquisite con il sistema di ripresa OSIRIS (Optical, Spectroscopic and Infrared Remote Imaging System) e precisamente con la Narrow Angle Camera (NAC), progettata per acquisire immagini delle superfice in alta risoluzione nelle lunghezze d'onda di NUV-VIS-NIR (Keller et al., 2007).

L'importanza della missione Rosetta risiede nel fatto che è stata la prima missione che si è prefissa come obiettivo principale lo studio ravvicinato del nucleo di una cometa, avvicinandosi nello specifico alla cometa 67P/Churyumov-Gerasimenko delle comete della famiglia di Giove, per effettuare una serie di orbite controllare attorno ad essa per consentirne l'osservazione e scortarla durante il suo passaggio al perielio ed è stata la prima missione che ha fatto atterrare un lander sulla superficie di un corpo cometario.

Le immagini acquisite da OSIRIS hanno permesso di descrivere un corpo cometario di forma bilobata con presenza di larghe depressioni, pits, scarpate, terrazze, cuestas, mesas, fratture, frane, stratificazioni continue e depositi di materiale fine (Sierks et al., 2015; Thomas et al., 2015). Studi sulla stratificazione hanno permesso di individuare su entrambi i lobi della cometa una stratificazione di tipo cipollare, la quale si deve essere formata

antecedentemente all'unione dei due lobi, avvenuta con una collisione a bassa velocità (Massironi et al., 2015; Davidsson et al., 2016).

Con lo scopo di identificare due involucri distinti della stratificazione di tipo cipollare e di verificarne le variazioni spettrofotometriche, sono state selezionate due sequenze di immagini multispettrali OSIRIS NAC acquisite successivamente al passaggio al perielio che inquadrano il lobo minore della cometa 67P. Tali immagini sono state sovrapposte per costruire dei cubi multispettrali ai quali sono stati applicate delle correzioni fotometriche per eliminare gli effetti dovuti alle diverse condizioni di illuminazione.

Ai cubi ottenuti è stata successivamente applicata una classificazione supervisionata Maximum Likelihood a due classi, le cui aree campione sono state selezionate sugli affioramenti consolidati identificati e i relativi depositi sulla base della riflettanza superficiale e dell'elevazione strutturale definita dal modello ellissoidale della struttura interna del nucleo cometario (Penasa et al., accettato).

La classificazione ha evidenziato la presenza di un involucro interno ed un involucro esterno (entrambi costituiti da più strati) con proprietà spettrali diverse, possedendo l'involucro interno maggiore albedo rispetto a quello esterno.

Tali differenze potrebbero essere dovute alle diverse proprietà tessiturali o a variazioni composizionali fra i due involucri.

Abstract

The international space mission Rosetta was approved in 1993 by the European Space Agency (ESA), within the program Horizon 2000 for the exploration of the minor bodies of the Solar System, and launched on 2 March 2004. The spacecraft was constituted by the Rosetta orbiter and the Philae lander, the latter projected to anchor at the cometary nucleus of the comet, collect images and perform superficial analyses. The mission concluded on September 2016 with the controlled landing of the probe on the comet.

The instruments onboard the spacecraft were chosen to perform a wide range of analyses, among which image analysis, spectroscopy and spectrophotometry. In particular, the images used in this work were acquired with the imaging system OSIRIS (Optical, Spectroscopic and Infrared Remote Imaging System) and precisely with the Narrow Angle Camera (NAC), projected to acquire high resolution images of the surface in the NUV-VIS-NIR wavelength (Keller et al., 2007).

The importance of the Rosetta mission lies in the fact that it is the first mission that set as main objective the close-range study of the nucleus of a comet, approaching specifically the comet 67P/Churyumov-Gerasimenko of the Jupiter-family comets. The spacecraft performed a series of controlled orbits around the comet, allowing its observation, and escorted it during its perihelion passage and, above all, was the first mission to land a lander on the surface of a cometary body.

The images acquired by OSIRIS allowed to describe a cometary body with a bi-lobed shape and with vast depressions, pits, scarps, terraces, cuestas, mesas, fractures, mass-wasting deposits, landslides, continuous stratifications and fine material deposits (Sierks et al., 2015; Thomas et al., 2015). Studies on the stratification allowed to detect on both lobes of the cometary nucleus a onion-like stratification, which should have formed previously the merging of the two lobes through a low velocity collision (Massironi et al., 2015; Davidsson et al., 2016).

With the aim to identify distinct envelopes of the onion-like stratification and to verify their spectrophotometric variations, two sequences of multispectral OSIRIS NAC images acquired after the perihelion passage and framing the minor lobe of comet 67P were selected. These images were overlapped to build two multispectral cubes to which were then applied photometric corrections to delete the effects due to the different illumination conditions.

To the cubes was successively applied a two-classes Maximum Likelihood supervised classification, on which the training areas were selected on the identified consolidated outcrops and relative deposits on the basis of the superficial reflectance and structural elevation defined by the ellipsoid-based model of the internal structure of the nucleus (Penasa et al., accepted).

The classification highlighted the presence of an inner and an outer envelope (each constituted by numerous stata) with different spectral properties, in particular with the inner shell brighter than the other one.

These difference could be due to different textural properties or to compositional variations between the two envelopes.

1. Minor planetary bodies: the comets

The observation of comets can be dated back to ancient times.

Over the millennia the mystery surrounding their origins and the unpredictable nature of their apparitions contributed to stoke the superstition that comets were herald of catastrophes, such as famines, plagues and wars, or that they preannounced the death of important people.

The real nature of the phenomenon has been uncertain up to the 18th century, when Edmond Halley (1656-1742) understood that comets are solid bodies belonging to our Solar System. Using equations of celestial mechanics, Halley demonstrated that the comets appeared in 1456, 1531, 1607 e 1682 were actually passages of the same comet with a period of about 75 years and he predicted its return in 1759, even if he didn't live long enough to witness the confirmation of his theory. However the comet was named after him and in 1986 it became the target of five different spatial missions, including the European Giotto mission (See ch. 2.1).

The development of new observational techniques and the following apparitions of comets Hyakutake and Hale-Bopp, respectively in 1996 and 1997, provided scientists with a vast database, which had been later enlarged and enhanced by the data concerning the missions Deep Space and Stardust up to the international spatial mission Rosetta developed by the European Space Agency (ESA), whose goal was the rendez-vous with comet 67P/Churyumov-Gerasimenko (See ch. 2.2).

1.1 The importance of comets

Comets are leftovers of a vast distribution of solid bodies that accreted in the protoplanetary disk during the early stages of formation of the planetary system. These small bodies have been widely described as the most primitive

and best-preserved materials of the Solar System, namely representative samples of the primordial planetesimals, accreted in the solar nebula and preserved at cryogenic temperatures and low pressures since the formation of the Sun. Therefore they are thought to have changed very little since their formation and are considered the most representative materials of the conditions present at the birth of the Solar System about 4.6 billion years ago (Brownlee D.E., 2005).

Their study can allow us to answer to the open questions concerning the accretion processes in the solar nebula and their variations with time and heliocentric distance, the chemical and physical conditions, such as composition, temperature and pressure, present during the formation of planetesimals and the actual composition of cometary nuclei that also drives the periodic activity.

Comets are very complex planetary bodies subjected to periodic activity of sublimation that cause the formation of a coma and a tail, made up of gas and dust materials, which can provoke orbital, compositional and mass variations. According to the International Astronomical Union (IAU) is the presence or absence of this periodic activity that defines the difference between comets and asteroids. Although they differ for provenance, size and orbit, it is their different composition that cause the establishment of cometary activity when the comet approach the Sun. In fact, with respects to asteroids, mainly composed of rocks and metals, comets contain, along with rocks, a lot of ice which sublimates when heated by the solar radiation.

Understanding the complexity of a comet as a whole is an arduous challenge to which the planetary sciences have devoted several space missions over the past few years, with the aim to increase the knowledge of the physico-chemical and geological processes that had been influencing and modelling these bodies which have been witness to important Solar Systems evolution events.

1.2 Origins and reservoirs

The protoplanetary disk was originally made up of gas and dust material which, aided by turbulent gas streams, rapidly began to accrete growing in size until the formation of the planetesimals, and thus of the planets nuclei.

Around 3 million years, this rapid initial growth phase, due to the gravitational force too weak to collect more material, left in the outer part of the solar nebula pebbles of icy and rocky materials that started a low velocity accretion process which led to the formation of brittle planetary bodies with high porosity and low density, namely comets and asteroids (Davidsson et al., 2016).

Although merging events may have happened on smaller scale, comets have been substantially unaffected by gravitational compression because of their small size and low density, thus their nuclei morphology can either reflect the early accretionary processes and/or the following events of collision and erosion, both by sublimation and space weathering. Moreover, this slow growth, occurred in a span of time about ten times longer the one needed for the planets nuclei to form, also allowed comets to preserve their composition and thus they are thought to be the best representative samples of the oldest volatile compounds and primordial refractory materials from the solar nebula: therefore they can be considered fossils of the nascent Solar System.

Over the next 25 million years, the mild increase in collision velocities caused by the stirring of the cometary orbits led to the formation of denser external layers on the cometary nuclei and made possible the collision between few kilometer-sized bodies, which gently bumped into each other, thanks to the dynamical coldness of the primordial disk that guaranteed the survival of both comet nuclei, leading to the formation of bi-lobed comets, such as 19P/Borrelly and, above all, 67P/Churyumov-Gerasimenko (Davidsson et al., 2016) (See ch. 3).

Precisely the data obtained by the international space mission Rosetta and by its recon of comet 67P/Churyumov-Gerasimenko have permitted to resolve the query concerning the primordial or collisional nature of comets, which counterpose ancient leftovers of the protoplanetary disk to welded fragments resulting from collisions with others larger bodies. The analysis of data acquired by the spacecraft Rosetta regarding physics, morphology and composition of the cometary nucleus identified a body with low bulk density, high porosity, negligible tensile strength, extensive stratification along with large abundances of supervolatiles compatible with an origin of comets as primordial survivors of the Solar System (Morbidelli & Rickman, 2015; Davidsson et al., 2016).

All cometary bodies formed beyond the snow line of the solar nebula, where conditions were sufficiently cold to allow water ice condensation. However, comets formed in environments with significantly temperature variations: some formed in the quite warm regions near Jupiter's orbit, where the temperature may have been greater than 120 K, while others formed beyond Neptune's orbit where the temperatures probably were less than 30 K. Comet are thus a mix of nebular and pre-solar materials accreted over a vast range of distances from the Sun in settings that differed in temperature, pressure, erosional and accretional mechanisms (Brownlee D.E., 2005).

The cometary bodies formed within a few astronomical units from the Sun, due to the proximity of the giant planets, and in particular of Saturn (Fernández J.A., 1997), were successively thrown out the Solar System, gathering themselves into the Oort Cloud (Oort J.H., 1950). The other comets, formed between 30 and 100 AU from the Sun, not affected by these perturbations, instead, remained in situ constituting the Edgeworth-Kuiper Belt and its associated Scattered Disk.

Oort Cloud and Edgeworth-Kuiper Belt are therefore the main reservoirs of comets, into which they are stored in appropriate segregation from the solar heating and the planetary perturbations (Fig. 1).

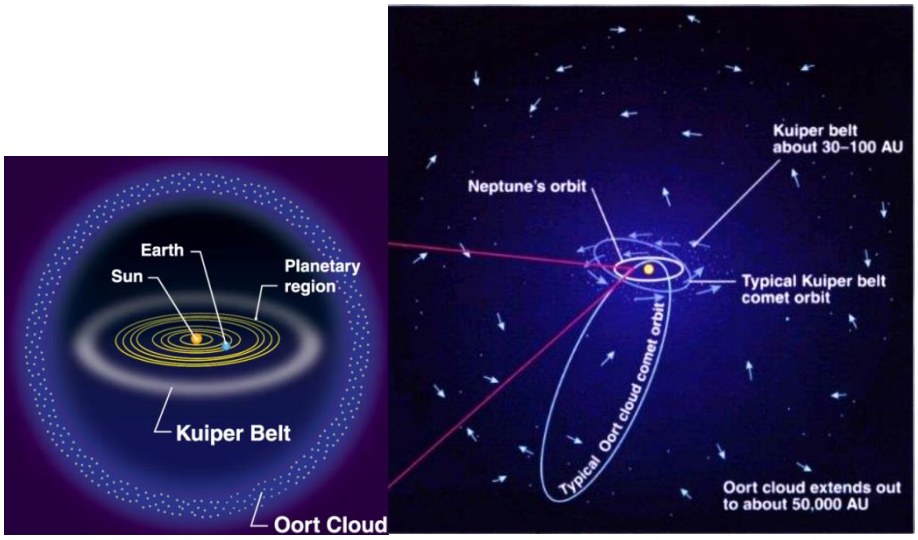

Fig. 1 Representation of cometary reservoirs and their typical comet orbits.

The Kuiper Belt speculated by Kenneth Edgeworth (1880-1972) and Gerard Kuiper (1905-1973) in the 1950s and then validated by Dave Jewitt e Jane Luu in 1992 with the discovery of the first Trans Neptunian Object (TNO), is a disk-like structure lying on the ecliptic, located beyond the Neptune's orbit and that extend itself between 30 and 50 AU from the Sun, even if the external limit is not clearly defined, and it is included in the innermost part of the Scattered Disk, which stretches between 30 and 100 AU.

This region was supposed by Kuiper to try to explain the presence of some comets that circulate in the Solar System into periodic orbits with very short orbital periods before rapidly sublimate in few hundreds of thousands of years. These comets, defined as short period comets, cannot be present in those orbits since the formation of the Solar System: Kuiper's solution was to hypothesize a population of primitive cometary bodies preserved from the original planetesimals, stored beyond the orbit of Neptune and occasionally injected in the inner Solar System due to gravitational interaction by the giants planets.

The Oort Cloud, instead, is a isotropic nearly spherical reservoir extended between 10 000 and 50 000 AU that surround our Solar System. Its presence was supposed by Jan Hendrik Oort (1900-1992) in 1950 to try to

explain the presence of new long-period comets coming from regions beyond 50 000 AU, without a predominant direction and not of interstellar origin, since they share the same motion of the Sun. These should be injected into the inner Solar System principally because of the tidal effects due to gravitational perturbations and to the close-range passage of stars and molecular clouds (Oort J.H., 1950; Delsemme A.H., 1987; Wiegert & Tremaine, 1998). The extension and the cometary population of the Oort Cloud are still too uncertain, indeed, it remains one of the lesser-known regions of the Solar System.

The perturbations that provoke the injection of new comets from the different reservoirs usually does not modify the orbit of the cometary body: this allow thus to distinguish comets coming from the Kuiper Belt or the Oort Cloud.

1.3 Classification

Cometary bodies are generally classified on the basis of their orbital period into long-period or short-period comets, depending on whether this is greater or lower than 200 years. This limit has historical justification since it allowed to relate over the time comets' apparitions with orbital period lower than 200 years (Levison H.F., 1996).

Short-period comets are divided into two groups. Comets with orbital periods smaller than 20 years and low inclinations are called Jupiter-family comets, since they tend to have the aphelion near the orbit of this planet. Comets with orbital periods between 20 and 200 years and more inclined orbits are instead called Halley-type comets.

All the comets near the Sun and that show cometary activity have a short life, since they are on instable orbits, that are easily perturbed by the planets, and at each passage near the Sun they are rapidly impoverished in volatile elements up to their fragmentation.

Long-period comets, instead, have orbital periods from 200 up thousands or even millions of years with very eccentric and casual orbits, with the aphelion that can be far beyond Neptune's orbit. Long-period comets are also typically divided into two main groups, based on the distribution of their semi-major axis *a*.

Whereas a comet with semi-major axis greater than 10 000 AU at its first passage in the Solar System is unlikely to maintain the same value during the successive passages, due to the gravitational kicks received by the proximity of the planets and the Sun, it is possible to distinguish new and returning comets on the basis of this value. Therefore comets with a>10 000 AU are considered new comets from the dynamical point of view, while cometary bodies with a<10 000 AU are called returning comets, because they have already passed through the planetary system (Fig. 2).

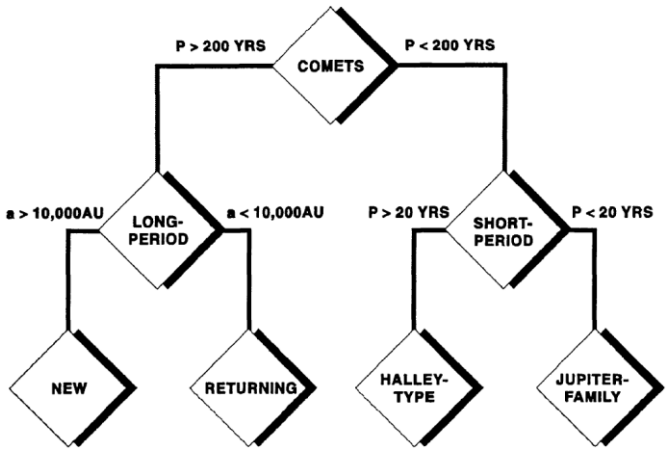

Fig. 2 Historical comets classification (Levison H.F., 1996).

However these limits considered arbitraries and without physical basis led to a new more objective classification based on the Tisserand parameter T_J (Levison H.F., 1996), on which are considered the semi-major axis *a* of the cometary body, its eccentricity *e* and inclination *i* with respect to the orbit of a perturbing larger body, and the semi-major axis a_J of this body (Fig. 3).

$$T_J = \frac{a_J}{a} + 2\sqrt{\left[(1-e^2)\frac{a}{a_J}\right]}\cos(i)$$

Fig. 3 Tisserand parameter.

In this way it is possible to distinguish ecliptic comets, with $T_J>2$, and nearly isotropic comets, with $T_J<2$. The first ones are further divided into three groups, allowing to distinguish the Jupiter family comets, with $2<T_J<3$, and the cometary bodies with $T_J>3$ which in turn are subdivided in Encke-type comets, if their orbit is interior to that one of Jupiter, and Chiron-type comets, if their orbit is exterior to the Jovian one.

The nearly isotropic comets are distinguished, as before, in new and returning comets. The latter are further subdivided into Halley-type comets, if they have a semi-major axis sufficiently small to be trapped by the resonance motion of the giant planets, or in external comets, if they have a semi-major axis greater than 40 AU, a boundary determined with respect to Pluto's semi-major axis (Fig. 4).

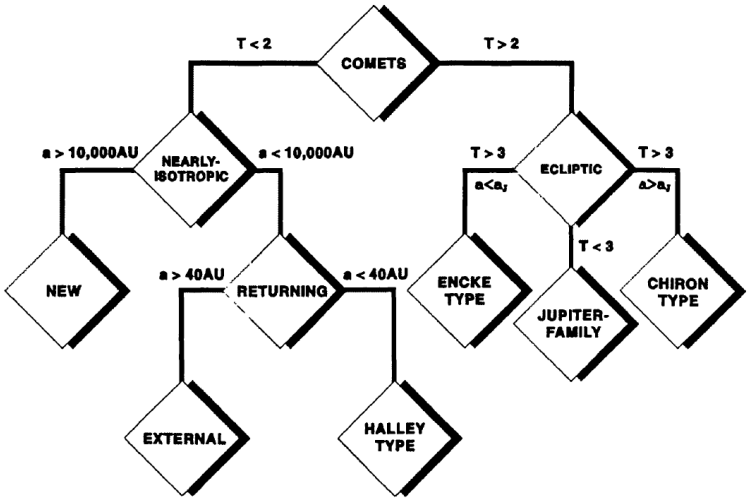

Fig. 4 Comets classification based on Tisserand parameter (Levison H.F., 1996).

These new classes are meaningful from the dynamical point of view and therefore they could reflect the origin of the comets they group. Indeed, it is believed that the majority of the nearly isotropic comets originated in the Oort Cloud, that is thus considered the reservoir of the Halley-type and long-period comets in general, while the majority of the ecliptic comets originated in the Kuiper Belt, considered the Jupiter family comets' reservoir.

1.4 Physical properties and evolution

Comets are minor planetary bodies made up mainly of ices, organic materials and silicates.

The first model of a cometary nucleus described comets as "sandbanks", namely a totality of meteoric material naturally porous, not necessarily gravitationally bonded and containing large quantities of molecular gas (Lyttleton R.A., 1948). This model was successively substituted by the "dirty snowball" model, suggested by Fred Whipple (1906-2004) in 1950 and confirmed by the images of Halley's comet acquired by the probe Giotto in 1986. Whipple described comets as conglomerate of water ice and dust mixed to volatile material (Whipple F.L., 1950). The following missions confirmed the presence of a shell of refractory materials on the cometary aggregate correctly revealed by Whipple. Compared to the previous one, this model allowed to explain how a cometary body could pass close to the Sun without entirely volatilize itself, thanks to the thermic shelter offered by the refractory coating, and to solve the phenomenon of delay or anticipation of the perihelion passage due to the "rocket-effect", namely to the release of gas in anti-solar direction that accelerates the comet in the direction of the orbital motion.

Cometary nuclei have variable sizes that can be derived by photometric analysis on visible wavelength when comets are afar from the perihelion or by thermal emissions analysis on infrared and microwave wavelength. In general, cometary nuclei range in size between hundreds of meters and tens of kilometers, and are mainly made up of ices, of water, carbon monoxide and carbon dioxide, and of rocky materials, such as amorphous or crystalline silicate refractory minerals and carbonaceous materials.

Commonly it is believed that a comet can be constituted by only one solid irregular nucleus or by a chaotic agglomerate of primordial cometesimals, called "rubble pile", accreted inside the solar nebula or welded by collision. This structure is consistent with the extremely low density calculated for the cometary nuclei, ranging between 0.5 and 1.2 g/cm^3 (Weissman et al., 2004).

Comparting these values with the density of water, 1 g/cm^3, and the density of the silicate and carbonaceous materials, about 2-3 g/cm^3, it is possible to infer that comets are extremely porous bodies with a porosity ranging between 75-88%, as confirmed by the analyses of the impact crater created by the Deep Impact collisional experiment on comet 9P/Tempel 1 (Ernst & Schultz, 2007).

When comets are inactive they behave as asteroids and are influenced by the same processes, such as orbital resonances, solar radiation pressure, fragmentation and collision.

During the approaching of the Sun, instead, at distances generally lower than 3 AU, the volatile materials, in particular water ice and carbon dioxide, begin to sublimate impoverishing the comet and leading to the formation of a wide temporary atmosphere, called coma, that surround the cometary nucleus, and one or two tails, made up respectively of dust and ions.

The presence of coma and tails is indicative of a comet defined active: when present, their brightness exceed by far the reflectance of the cometary nucleus, while if absent the comet's luminosity is only due to the reflection of the solar light by the body (Fig. 5).

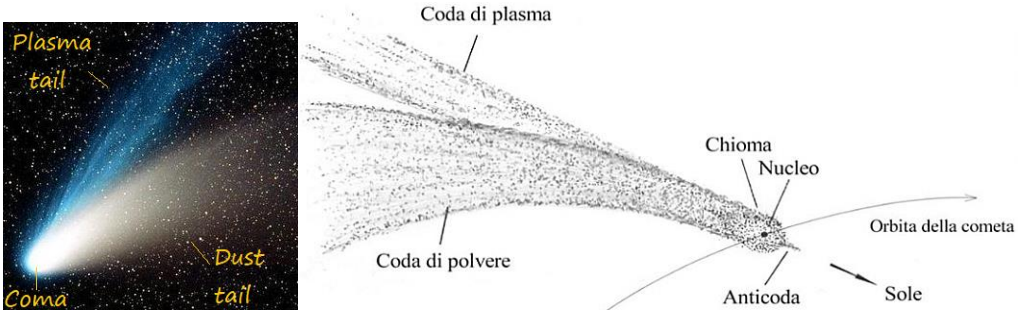

Fig. 5 Realistic (*on the left*) and schematic (*on the right*) representation of a comet.

The coma of a comet is a dense cloud essentially made up of gas and dusty materials due to the sublimation of ices on the comet's surface. It has a spherical slightly oblate shape that can reach diameters of about 10^4-10^7 km, based on the distance from the Sun and its chemical composition.

Water, carbon dioxide, methane, ammonia and other complex molecules, freed by the sublimation of the nucleus, compose the so-called parent molecules that constitute the inner coma.

The visible coma, even at naked eye, is instead made up of neutral radicals, defined as daughter molecules, obtained by chemical reactions such as photodissociation and photoionization. These reactions and the charge exchange with the solar wind finally lead to the formation of the atomic coma, also known as hydrogen crown.

The solid component of the coma, instead, is made up of small icy and rocky grains freed by the sublimation. When the solar radiation and wind interact with the coma, these grains are pushed elsewhere giving rise to the dust tail.

The coma, being not gravitationally bounded to the nucleus is a temporary phenomenon that varies in function of the distance from the Sun and the cometary orbit (Fig. 6).

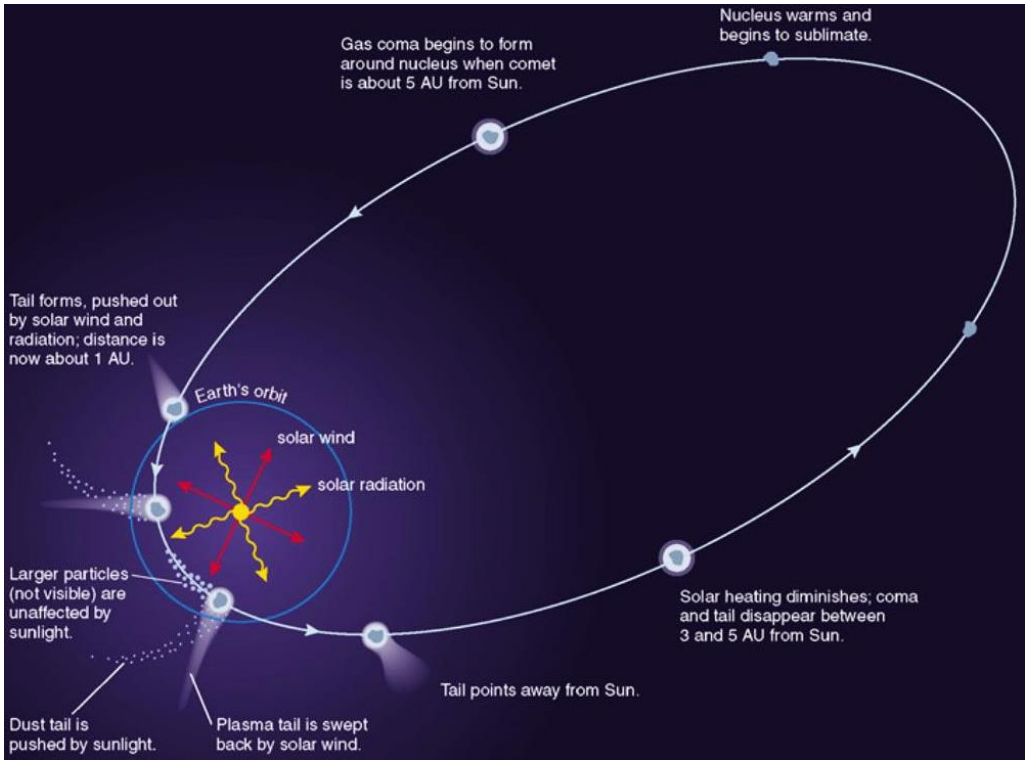

Fig. 6 Cometary activity development approaching the Sun and plasma and dust tails trajectory representation.

In a comet it is possible to identify two types of tails: the dust and ions tails. The first one is made up of icy and rocky grains present in the coma and pushed in opposite direction to the Sun by the solar radiation pressure. It can extend up to 10^7 km in an antisolar trajectory with curvilinear course that follow the cometary orbit (Fig. 6).

The ion (or plasma) tail, is instead made up of gasses present in the coma that interacting with the interplanetary medium, namely the charged particles transported by the solar wind, ionize themselves. As the dust tail, also the plasma one extends up to 10^7-10^8 km following the solar wind motion in opposite direction to the Sun, anyway it maintains a rectilinear course (Fig. 6) and, based on the polarity change of solar magnetic field, it can detach itself from the comet, as happened to comet Hyakutake on 24 March 1996 (Fig. 7).

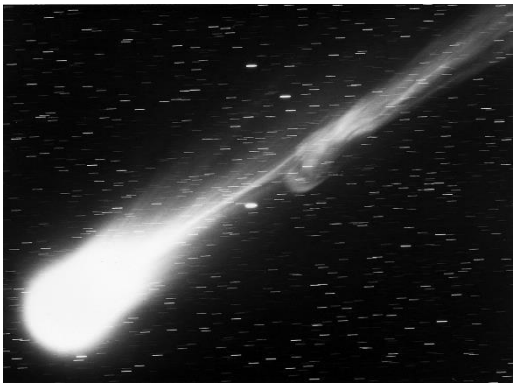

Fig. 7 Comet Hyakutake's plasma tail detachment on 24 March 1996.

Not always the cometary activity is well distributed on the surface of the body: indeed, it is often possible to have only some areas temporarily actives and responsible for the degassing.

The presence of inactive regions and the general weakness of the tails of short-period comets are explained through the mantle refractory mantle according to which the repeated passages near the Sun lead to the formation of a superficial coating of silicate-carbonaceous refractory materials that prevent the sublimation of volatile materials hampering the cometary activity.

A comet can cease its activity for depletion of sublimational volatile materials and become therefore an asteroid with a stable orbit, otherwise can

collide with other planetary bodies or fragment itself due to the gravitational pushes from the Sun and Jupiter, on which can then crash-landing, as happened to comet Shoemaker-Levy 9 that broke apart because of the interaction with Jupiter in 21 fragments then fell onto the planet on July 1994 (Fig. 8).

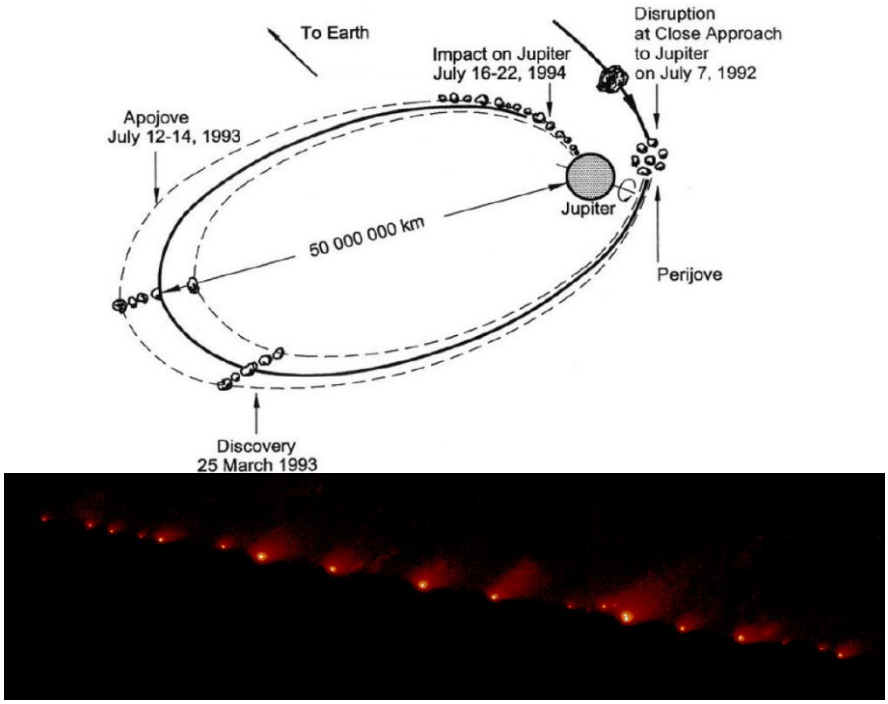

Fig. 8 Comet Shoemaker-Levy 9 fragmentation because its interaction with Jupiter on 7 July 1992 and successively impact two years later.

1.5 Composition

As previously introduced, a comet is essentially made up of volatile, refractory and organic materials.

The most abundant volatile component is the ice of H_2O. Molecules such as CO_2, CO, O_2 and N_2 can be found both mixed with ice and trapped in clathrates. Each compound, indeed, condenses, or sublimes, at different distances from the Sun, defined as snow lines. In particular, the snow lines of H_2O and CO_2 are respectively at about 5 and 12 AU: carbon dioxide sublimes at temperatures of only 80 K while the water at about 180 K. This imply that

extremely volatile compounds such as CO and CO_2, if trapped in solid state by the water ice matrix, will tend to sublimate at temperatures greater than normal.

The sublimation of volatile materials is prevented, at least partially, by the superficial coating of refractory materials. These materials are made up of a mix of aromatic and aliphatic organic compounds with C-H bonds containing N, such as glycolaldehyde (CH_2OHCHO), hydrogen cyanide (HCN) and formamide ($HCONH_2$), and of silicates, such as pyroxenes, forsterite and anorthite, present both in crystalline or amorphous form (Asadi et al., 2015). Since the condensation temperatures of these minerals are extremely elevated (1200-1400 K), at the time of their formation they probably were too close to the Sun and were transported beyond the snow line at a later stage to be included into the cometary nucleus.

The sublimation processes concern first of all the superficial ices. However, even the deepest ices contribute to the impoverishment of the cometary body. Their sublimation, indeed, would be facilitated by the presence of exposed scarps and by the energetic processes with consequently released of heat, as the destabilization of clathrates and the crystallization of water ice (Vincent et al., 2015). The volatilization of these sublayers can generate a system of inner cavities and lead to superficial collapses, provoking the rapid exposition of new fresh ices, they too subjected to sublimation and responsible for the production of jets.

The presence and provenience of organic and water molecules on Earth is still an open question concerning the origin and evolution of the Solar System. One of the main theory affirms that these molecules were brought to Earth through cometary impacts.

To try to explain their origin on Earth it has been used the isotopic ratio between deuterium and hydrogen (D/H). This ratio shows a great variability among the planetary bodies starting from the lower value of Jupiter's atmosphere ($2.1 \pm 0.5 \times 10^{-5}$), similar to the interstellar ratio and considered the best representative value of the proto-Sun, to the six times greater value of the terrestrial planets, to the extremely high values of long-

period comets, with enrichment up to twenty times greater the proto-solar value. Exceptions to this enrichment trend from the Sun toward the outer Solar System are the values of the Jupiter family's comets, which show a vast heterogeneity. Only the D/H value of comet 103P/Hartley 2 ($1.6\pm0.24 \times 10^{-4}$) was found to match the composition of Earth's water (1.5×10^{-4}), while the D/H ratio measured by the ROSINA instrument (Rosetta Orbiter Spectrometer for Ion and Neutral Analysis) for comet 67P/Churyumov-Gerasimenko ($5.3\pm0.7 \times 10^{-4}$) is three times greater than that for Earth's oceans and, in general, higher than measured of any Oort Cloud comet as well (Fig. 9). This confirms the different origin of comets, formed over a wide range of distances from the Sun, and nevertheless put under debate the contribution of comets for the presence of water on Earth (Altwegg et al., 2014).

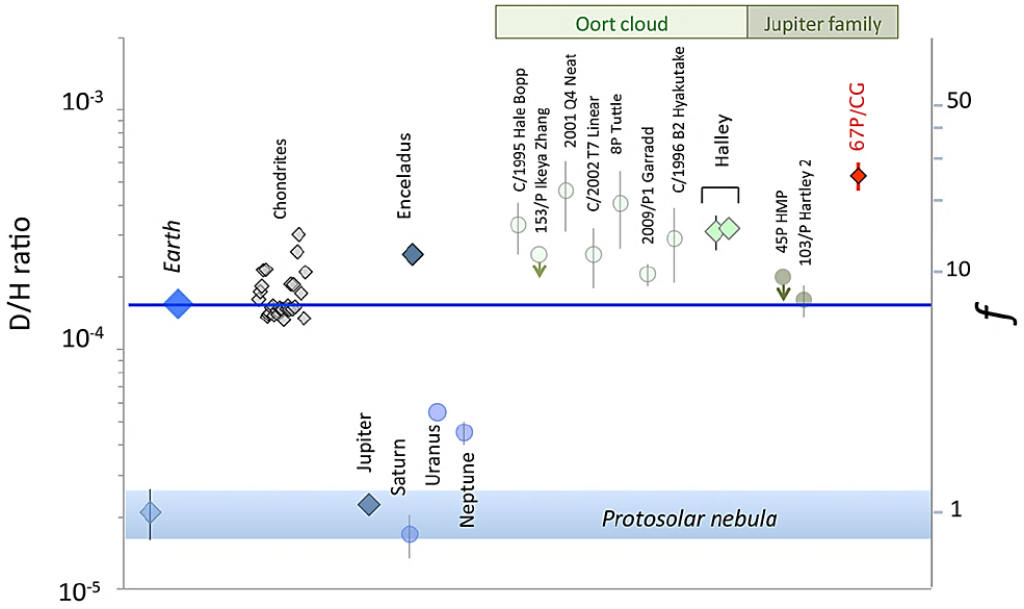

Fig. 9 D/H ratio in different objects of the Solar System (Altwegg et al., 2014).

2. Space missions

Stars have been objects of contemplation, veneration and study from many civilization over the course of human history. However, these first observations were made with naked eye.

Only in 1608 the invention of the telescope by Hans Lippershey (1570-1619) provided a real breakthrough in the astronomic studies, allowing Galileo Galilei (1564-1642) to validate the heliocentric model, previously enunciated by Niccolò Copernico (1473-1543), and to carefully observe the celestial bodies.

Over the centuries the scientific progresses have led to the invention of optical and radio telescopes increasingly sophisticated for the observation of the sky from Earth and of orbital telescopes located beyond the terrestrial atmosphere. Nevertheless these observations still present considerable restrictions in terms of maximum spatial and spectral resolution achievable. Only close-up observations through spatial probes can grant a complete study of minor bodies such as comets and asteroids.

The direct spatial exploration allows to study a comet with different angle and illumination conditions and, above all, to observe it when it is still inactive and invisible from Earth. In this way it becomes possible to study the shape and size of cometary nuclei, to distinguish the morphologic features and the compositional heterogeneity of the surfaces, to identify the active areas and to supervise the onset of cometary activity which leads to the formation of jets and coma.

2.1 History of cometary space missions

The direct exploration history of comets begins with the close-range passage of the famous comet 1P/Halley in 1986. This was the most copious and

extensive space investigation occurred in such a short span of time, enough to be described as “Halley Armada”. This fleet was made up of a probe by the National Aeronautics and Space Administration (NASA), two probes by the Institute of Space and Astronautical Science (ISAS) of Japan, two probes developed jointly by Russian and French and a probe by the European Space Agency (ESA).

The spacecraft ICE (International Cometary Explorer) by NASA, after the conclusion of its mission for the study of the Earth’s magnetic field and of the solar wind, was redirect firstly to pass near the plasma tail of comet 21P/Giacobini-Zinner on September 1985 and later to meet up with comet 1P/Halley on 28 March 1986, at a distance of about 31 million of kilometers from the cometary nucleus.

The twin probes Sakigake e Suisei by ISAS, launched in 1985, were the first Japanese spatial missions to exit the Earth system and to approach the Halley’s comet respectively on 11 March 1986 at a distance of about 7 million of kilometers and on 8 March 1986 at 151 000 km.

The spacecraft Franco-Russian Vega-1 and Vega-2 launched on December 1984, after the release of their own lander of the surface of Venus during their journey, succeeded to approach comet 1P/Halley respectively on 6 March 1986 at a distance of 8890 km and on 9 March 1986 at 8030 km.

Despite the good result gained by the Franco-Russian team with respect to the American and Japanese colleagues, the probe that succeeded to come nearer to the target was the spacecraft Giotto by ESA.

The probe Giotto, launched on 2 July 1985, is named after the Medieval painter Giotto who took inspiration from the passage of the Halley comet in 1301 to draw the guiding star of Bethlehem in the nativity of the Cappella Scrovegni in Padua (Fig. 10). On 13 March 1986, the spacecraft passed at a distance of only 596 km from the famous comet, collecting the first closed-up images of a cometary nucleus and allowing to reveal their real nature. The images, more or less 2000 shot by the Halley Multicolor Camera right before it was destruct by an impact with material ejected by the comet

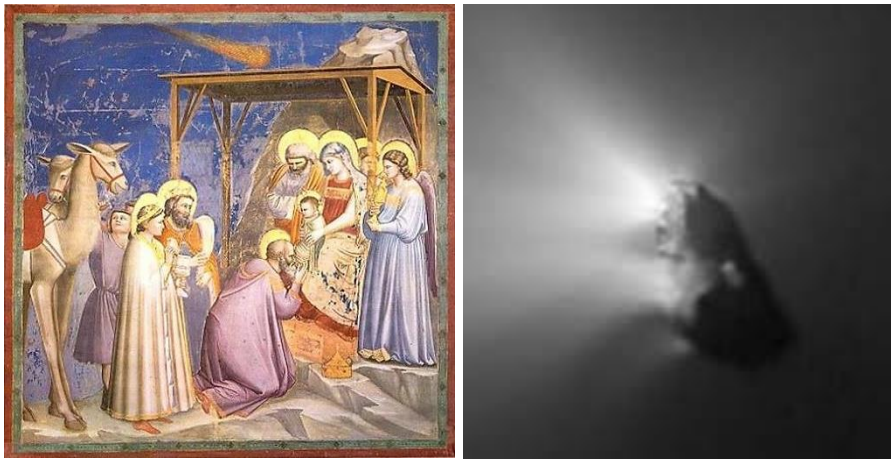

Fig. 10 Giotto's representation of Halley's comet as the guiding star of Bethlehem in the nativity of the Cappella Scrovegni in Padua (*on the left*) and the cometary nucleus of 1P/Halley as shot by the Halley Multicolor Camera (*on the right*).

itself, showed a dark, irregular, elongated and vaguely bi-lobed object, similar to a potato, with only some active areas which released jets of gas and dust into the space, and a very porous and low density structure (Fig. 10). Thanks to these images Whipple's model of the "dirty snowball" was finally validated, pointing out that maybe was more important the "dirt" (i.e. refractory material mainly organic) with respect to the "snow" (ices of H_2O, CO_2 and CO). The spacecraft Giotto was successively hibernated and woke up to meet up with a second comet. On 10 July 1992, indeed, Giotto passed at about 200 km from comet 26P/Grigg-Skjellerup, picking up information about its coma ambient.

The following encounters with a comet concern spatial missions promoted by NASA.

The first was the mission Deep Space 1, launched on 24 October 1998, whose primary target was to test 12 new advanced technologies. During its journey, the probe passed in the immediate vicinity of the asteroid Braille performing analysis of its composition and the potential presence of a magnetic field and, on 22 September 2001, it succeeded to pass at about 3500 km from comet 19P/Borrelly, carrying on a survey of its cometary nucleus.

The spacecraft Stardust launched on 7 February 1999 was the first probe to capture and bring back to Earth fragments of cometary material. On 2

January 2004, in fact, the spacecraft moved at less than 240 km from the nucleus of comet 81P/Wild 2 capturing about 2000 particles of cometary dust and sending them back on Earth, through a capsule, on 15 January 2006, where they were analyzed allowing the identification of minerals such as olivine, diopside and anorthite. The high resolution images collected by the Navigation Camera, moreover, permitted a tridimensional reconstruction of the nucleus to allow its morphological and compositional study. The mission was successively extended to approach comet 9P/Tempel 1, also target of the spatial mission Deep Impact, allowing thus to study the changes occurred after the passage at perihelion.

Among these successes there is also a failure, and it concerns the spatial mission Contour. It was lauched on 3 July 2002 with the aim to perform a detailed study of the nucleus of two different comets, 2P/Encke and 73P/Schwassmann-Wachmann 3. Anyway, on 15 August 2002, the contact with the spacecraft was lost after an engine fire during the manoeuvres to move it onto a heliocentric orbit.

On 12 January 2005 was launched the space probe Deep Impact. With respect to the previous missions, whose aim was mainly to approach, photograph and examine the comets' surface, the mission Deep Impact was planned to study the inner composition of a comet. After 174 days of journey, the probe reached its target, the comet 9P/Tempel 1, and shot a copper projectile of 370 kg that, impacting on the surface of the cometary body, excavated a crater of 100 m of diameter and lifted a cloud of fine materials that caused the exposition of the underlying fresh material, whose brightness decreased with the progressive dissipation and fall-out of dusty materials. The analysis of the comet's interior and surface composition allowed to determine the presence of silicates, clay, carbonates, water ice, iron-bearing compounds, aromatic hydrocarbons and a substantial amount of organic material and to assert that the ice and other materials deep within the cometary nucleus are well shielded from solar heating and thus may be unchanged from the early days of the Solar System. Successively the mission was extended, renamed

EPOXI and authorized for a new journey to another comet, 103P/Hartley 2, reached on 4 November 2010.

The last space mission whose aim was the closed-up encounter with a comet was the mission Rosetta of the European Space Agency, launched on 2 March 2004 and ended on 30 September 2016 with the controlled landing of the probe on the surface of its target, the comet 67P/Churyumov-Gerasimenko.

2.2 Rosetta mission

The international space mission Rosetta was approved in 1993 by the European Space Agency (ESA) within the program Horizon 2000 for the exploration of the minor bodies of the Solar System and launched on 2 March 2004.

The mission bears the name of the famous Rosetta Stone, a piece of an ancient granodiorite stele found in 1799 by the French troops of Napoleone Bonaparte in a city of the Nile Delta, whose western name is Rosetta, and that is actually located at the British Museum of London (Fig. 11).

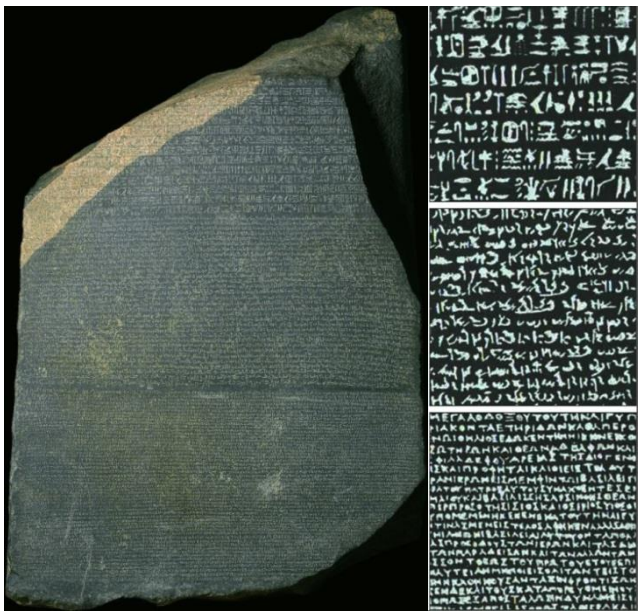

Fig. 11 The Rosetta Stone and the enlargement of its section in hieroglyphic, demotic and ancient greek (*from above*).

The stele reports the inscription of a Ptolemaic decree issued in 196 b.C. and divided into three sections in different scripts, namely hieroglyphic, the first script used by Egyptians, demotic, the evolution of the Egyptian script, and ancient greek, spoken by the ruling dynasty (Fig. 11). Since it is the same text, the stele offered the possibility to the French linguist Jean-François Champollion (1790-1832) to decipher the Egyptian hieroglyphics, recognizing them as a script at the same time figurative, phonetic and symbolic. Determining was the posthumous discovery of two well-preserved obelisks recovered at the Philae island in 1815 that allowed to validate the translation activity of the famous linguist.

Just as the Rosetta Stone and Champollion's work were fundamental to comprehend the history of the Ancient Egypt and its civilization, in other words three thousand years of history no one knew basically anything about, the spacecraft Rosetta and the lander Philae are helping to comprehend comets' nature and their rule on the primordial formation in our Solar System.

The importance of the space mission Rosetta lies in the fact that it was the first mission that has as ambitious goal the close-range study of the nucleus of a comet, specifically the nucleus of 67P/Churyumov-Gerasimenko, performing a series of controlled orbits and escorting it during its approach and perihelion passage. Moreover, it was the first mission to land a lander on the surface of a comet permitting to perform some in situ analyses.

The Rosetta mission, thus, allowed a characterization of the dynamic and physic properties of comet 67P, as well as a deepened study of the morphology and chemical composition of the cometary nucleus and coma.

During its journey, the spacecraft performed some flybys of the asteroids 2867 Steins and 21 Lutetia, permitting thus the study of bodies likewise ancient but more different in composition with respect to comets.

The data obtained from the Rosetta mission play a fundamental role in understanding the processes occurred during the early phases of our Solar System and its evolution, including the questions about the role of water and the origin of life on Earth.

2.2.1 Rosetta mission: timeline

The mission for the study of the minor bodies of the Solar System, and in particular for the study of comets, was for the first time take into account in the 1970s, but only on November 1993 was officially approved by ESA's Science Programme Committee.

Initially, the selected target was the periodic comet 46P/Wirtanen, anyway due to delays the launch was postponed and the choice thus dumped on another periodic guest of our Solar System, the comet 67P/Churyumov-Gerasimenko.

The spacecraft was launched with success from Kourou, in French Guyana, on board the Ariane-5G+ rocket on 2 March 2004, starting date of the ten-year expedition of the Rosetta probe (Fig. 12).

Fig. 12 Rosetta spacecraft's launch from Kourou on 2 March 2004 on board Ariane-5G+ rocket.

In order to gain enough orbital energy to reach its final target, Rosetta performed four gravity assist, one of Mars and three of Earth. The first Earth swing-by occurred on 4 March 2005 at a distance of about 1954 km above the Pacific Ocean, and was useful to determine the orbit and to check the instrumentations. Successively the probe directed toward Mars, realizing a gravity assist on 25 February 2007 at a distance of only 250 km from the planet's surface. During this passage, Rosetta faced successfully an unexpected

35 minutes eclipse that led to a black-out of the communications with Earth. Between the second and third Earth swing-bys, occurred respectively on 13 November 2007 and 13 November 2009, the spacecraft crossed the Main Asteroid Belt between Mars and Jupiter and on 5 September 2008 realized a flyby of asteroid 2867 Steins at a distance of 800 km, snapping its diamond shape and completing a first scientific objective in its journey toward comet 67P/Churyumov-Gerasimenko (e.g. Keller et al., 2010). On 10 July 2010 Rosetta, after its last Earth gravity assist and returning in the Main Asteroid Belt to reach its target, realized a flyby of asteroid 21 Lutetia at a distance of 3162 km, revealing the presence of different impact craters on its surface, its partially differentiated nature and its geological and deformative history (e.g. Sierks et al., 2011).

To limit the fuel consumption and minimize the mission's operating costs, it was necessary to introduce an hibernation period, lasted two and a half years, between 8 June 2011 and 19 January 2014. During this period the spacecraft's solar panels were always pointed at the Sun to receive as much light as possible: moreover Rosetta reached its maximum distance from the Sun, about 800 million kilometers, and from Earth, about 1000 million kilometers.

On 20 March 2014 Rosetta succeeded to see in the distance comet 67P/Churyumov-Gerasimenko, and between May and August 2014 performed a series of manoeuvres to reduce its distance from the target, until it reached 100 km of distance on 6 August 2014, attainment date of the target (Fig. 13).

A preliminary study of the surface allowed to locate a possible landing site for the Philae lander, that was unhooked on 12 November 2014. It was the first time that a landing was attempted on a low gravity small body that moves at a velocity of tens of thousands of km/h.

The lander, because of a malfunction of the anchorage system, bounced three times before landing in an unfavorable position for the battery power supply, whose depletion determined the beginning of the hibernation in the night of 15 November 2014. For seven months there were only brief

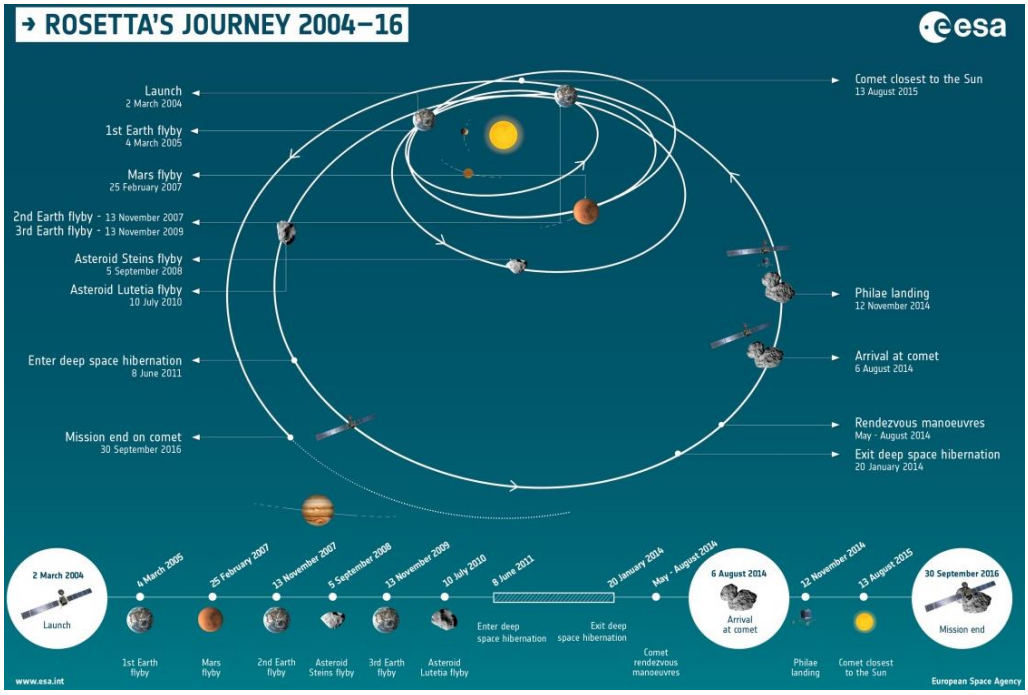

Fig. 13 Rosetta's twelve-years journey schematization.

contacts, during which Philae however succeed to send important data packets.

Escorting comet 67P/Churyumov-Gerasimenko during its approach to the Sun, Rosetta was able to monitor the changes of the cometary activity before and after the perihelion, reached on 13 August 2015, at a distance of 186 million kilometers from the Sun.

On 9 July 2015 the Philae lander sent its last message to the Rosetta probe, which continued its scientific investigations up to 30 September 2016, date of conclusion of the mission with a controlled landing of the spacecraft on comet 67P/Churyumov-Gerasimenko's surface (Fig. 14).

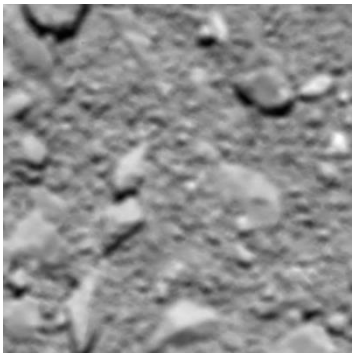

Fig. 14 Last image shot by the OSIRIS camera onboard Rosetta spacecraft.

2.2.2 Rosetta mission: orbiter

The Rosetta probe was constituted by an aluminium box with dimensions 2.8 m x 2.1 m x 2.0 m and by two wings long each one 14 m and covered by 64 m^2 of solar panels that could be rotated of ± 180° to catch as much light as possible. The total weight was equal to three tons.

Despite more than 50% of the weight was due to the propellant on board, Rosetta was the first probe to travel beyond the Main Asteroid Belt counting only on the solar panels for the power generation rather than the traditional radio-isotope thermal generators. To guarantee the survival of the instruments in the outer Solar System various layers of thermal insulating material were installed. For the close-range passage to the Sun, instead, were installed radiators to dissipate the heat in excess into the space and prevent the instruments overheating.

On one side of the orbiter was attached the Philae lander, designed to self-eject and anchor on the comet's surface, while on the other side was present a high-gain antenna of 2.2 m of diameter for the communications with Earth, and in particular for the spacecraft and instrumentations remote control and to send the data collected onboard. The radio communications between Rosetta and Earth occurred through the ESA's new deep-space antennas, parabolic antennas of 35 m of diameter that allowed to reach distances greater than 1000 million of kilometers, located in New Norcia, in Western Australia, and in Cerebros, in Spain. The signal took 50 minutes to reach the spacecraft, anyway not always was possible to have signal coverage, especially when Rosetta passed behind the Sun. Therefore the probe was provided both of an orbital control and stabilization system and of a wide memory that allowed to store the data until the following transmission period with Earth.

In order to study the nucleus and the gas and dust ejected by the establishment of the cometary activity, Rosetta was equipped with eleven instruments that combine remote sensing techniques, such as cameras and radio science measurements, and direct sensing systems, such as dust and particles

analyzer, mounted on the top of the probe in the Payload Support Module (PSM), while the subsystems were on the base in the Bus Support Module (BSM) (Fig. 15). They are here listed (Table 1).

Table 1 Rosetta spacecraft's instruments.

ALICE	Ultraviolet Imaging Spectrometer	Composition of nucleus and coma, noble gas and general abundances in coma and tail and production rates of H_2O, CO and CO_2 using extreme and far-UV spectral regions (70-205 nm)
CONSERT	COmet Nucleus Sounding Experiment by Radio wave Transmission	Tomography of nucleus using dielectric properties and propagation delay of radio waves between the instrument on the orbiter and the one on the lander
COSIMA	COmetary Secondary Ion Mass Analyzer	Secondary ion mass spectrometer with dust collector, primary ion gun and optical microscope
GIADA	Grain Impact Analyzer and Dust Accumulator	Scalar velocity, size and momentum of dust particles using optical grain detection system and mechanical grain impact sensor
MIDAS	Micro-Imaging Dust Analysis System	Microtextural and statistical analysis of cometary dust particles using atomic force microscopy
MIRO	Microwave Instrument for the Rosetta Orbiter	Near surface temperature, thermal and electrical properties of the surface using millimeter wave mixter receiver and submillimeter heterodyne receiver
OSIRIS	Optical, Spectroscopic and Infrared Remote Imaging System	High spatial resolution images of the nucleus, gas and dust using a dual camera imaging system operating in VIS, NIR and UV (250-1000 nm)
ROSINA	Rosetta Orbiter Spectrometer for Ion and Neutral Analysis	Two mass spectrometers and two pressure gauges for density and velocity data of the cometary gas
RPC	Rosetta Plasma Consortium	Five instruments to study physical properties of the nucleus, development of cometary activity and inner coma structure, dynamics and aeronomy
RSI	Radio Science Investigation	Spacecraft motion, perturbing forces acting and propagation medium using non-dispersive and dispersive frequency shifts, signal power and polarization of the radio carrier waves
VIRTIS	Visible and Infrared Thermal Imaging Spectrometer	Spectral mapping and spectroscopy using an imaging spectrometer

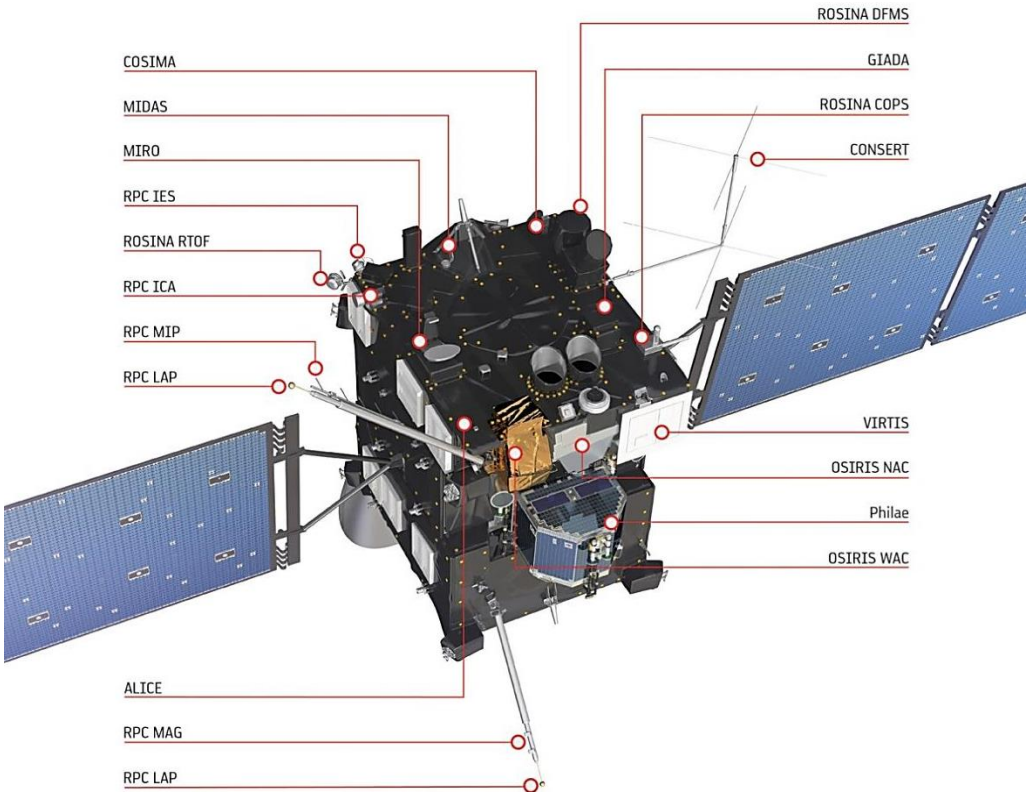

Fig. 15 Rosetta spacecraft's instruments.

2.2.3 Rosetta mission: lander

The Philae lander projected for the Rosetta mission, was constituted of a polygonal structure in carbon fiber with three foldable legs, for a total weight of at least a quintal. When the orbiter was well-aligned with the comet, the lander self-ejected from the spacecraft and opened its three legs both to soften the impact with the surface and reduce the possibility to bounce, both to rotate and lift itself up.

The lander was equipped with ten instruments, some of which were covered by solar panels to guarantee them a degree of autonomy, suitable to perform elemental, molecular, mineralogical and isotopic compositional analyses of the surface and to measure characteristic such as density, porosity and thermal properties (Fig. 16). They are here listed (Table 2).

Despite the final unfavourable landing position (in almost permanent shadow), that drastically reduced their capabilities, some instruments were able to obtain interesting results.

Table 2 Philae lander's instruments.

APXS	Alpha Proton X-ray Spectrometer	Chemical composition of landing site and potential alteration during Sun's approach
CIVA	Comet Nucleus and Visible Analyzer	Panoramic and microscopic imaging system for comet surface
CONSERT	COmet Nucleus Sounding Experiment by Radiowave Transmission	Radio sounding, nucleus tomography and internal structure with Rosetta orbiter
COSAC	COmetary Sampling and Composition experiment	Gas analyzer for elemental and molecular composition and complex organic molecules identification
PTOLEMY	Modulus protocol	Evolved gas analyzer for isotopic composition of light elements
MUPUS	MUlti-Purpose Sensors for Surface and Sub-Surface Science	Measurements of surface and subsurface properties
ROLIS	ROsetta Lander Imaging System	Imaging system
ROMAP	ROsetta lander MAgnetometer and Plasma monitor	Magnetometer and plasma environment monitor
SD2	Sampling Drilling and distribution subsystem	Drilling and sample retrieval
SESAME	Surface Electric Sounding and Acoustic Monitoring Experiment	Surface electrical and mechanical parameters, acoustic and dust impact monitoring

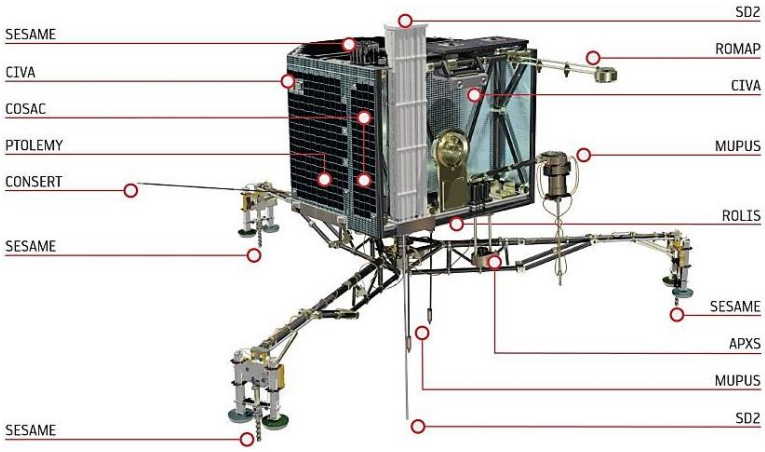

Fig. 16 Philae lander's instruments.

3. Comet 67P/Churyumov-Gerasimenko

Comet 67P was observed for the first time in 1969, when some astronomers of the Kiev Shevchenko National University went to the Alma-Ata Astrophysical Institute in Kazakhstan to conduct a survey of the cometary population. Klim Ivanovich Churyumov observing a photograph of comet 32P/Comas Solà (Fig. 17) shot by Svetlana Ivanovna Gerasimenko noticed an object similar to a comet, and after additional studies realized to have discovered a new comet, named after its discoverers in 67P/Churyumov-Gerasimenko (Lamy et al., 2007).

Comet 67P is one of the numerous short-period comets of the Jupiter family, namely those comets with orbital periods lower than 20 years and low inclination orbits coming from the Kuiper Belt but remained gravitationally trapped by the mass of this planet.

Studies on the orbital evolution of the comet (https://www.youtube.com/watch?v=SCSB1l8UHgA) demonstrated that up to 1840, comet 67P had its perihelion at 4 AU from the Sun (~600 million kilometers), a distance too large to be reached by the solar heat and that prevented the development of a coma and tail that would have made her visible from Earth. Only in 1840, a close encounter with Jupiter caused an orbital

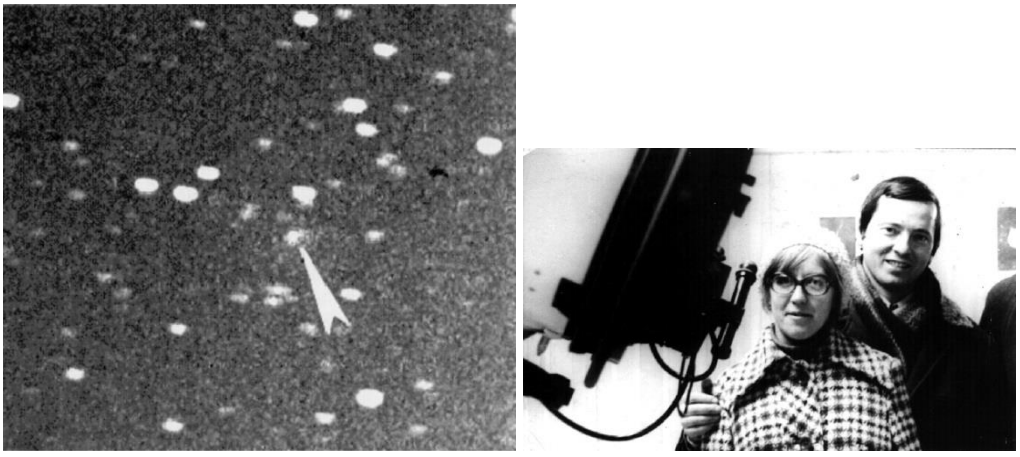

Fig. 17 Photograph of 32P/Comas Solà showing also comet 67P (*on the left*) and Klim Churyumov and Svetlana Gerasimenko on 1969 (*on the right*).

movement of the comet toward the interior of the Solar System, up to a perihelion distance of 3 AU (~450 million kilometers). During the following century, the perihelion distance gradually decreased up to 2.47 AU, and a successive close encounter with Jupiter in 1959 reduced the perihelion at the actual distance of 1.28 AU (~200 million kilometers). Comet 67P starting from 1969, year of the discovery, was observed form Earth on eight close encounter with the Sun, respectively on 1969, 1976, 1982, 1989, 1996, 2002, 2009 e 2015, with an orbital period of about 6.45 years (Lamy et al., 2007).

Comet 67P exhibits a bi-lobed shape, therefore it is possible to distinguish a larger lobe, called body, which has a size of about 4.1x3.3x1.8 km and a smaller lobe, called head, of about 2.6x2.3x1.8 km connected by a narrow region, called neck (Sierks et al., 2015) (Fig. 18).

Although the factors that contributing to the different cometary nuclei shape are still largely unknown, the particular shape of 67P suggests that it may be the result of the union of two distinct bodies once separated. From a morphological point of view, indeed, it is possible to identify thick set of strata (≤650 m) that individually envelope the two lobes (Fig. 18). Presumably this layering, defined "onion-like" stratification, formed during the accretionary phase of the lobes to witness that, even if previously separated, both experienced similar evolutionary history in the early stages of formation of the

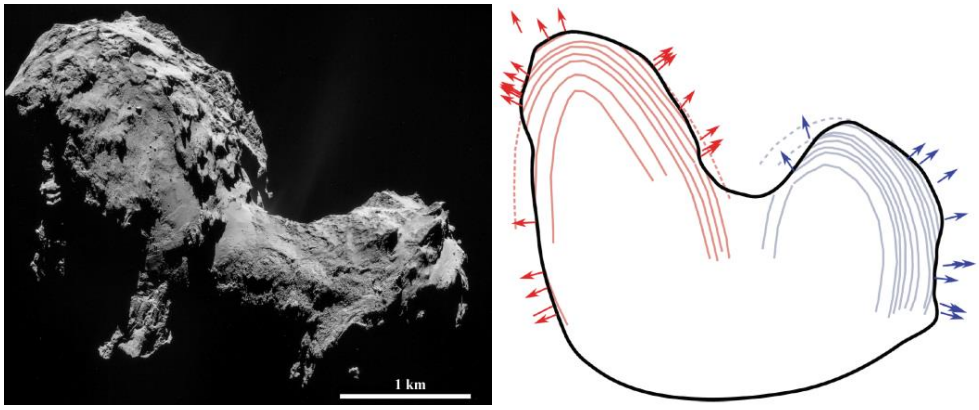

Fig. 18 Comet 67P/Churyumov-Gerasimenko nucleus' bi-lobed shape (*on the left*) and geological section of the comet with the interpreted inner stratification and arrows indicating the perpendicular to strata and terraces (*on the right*).

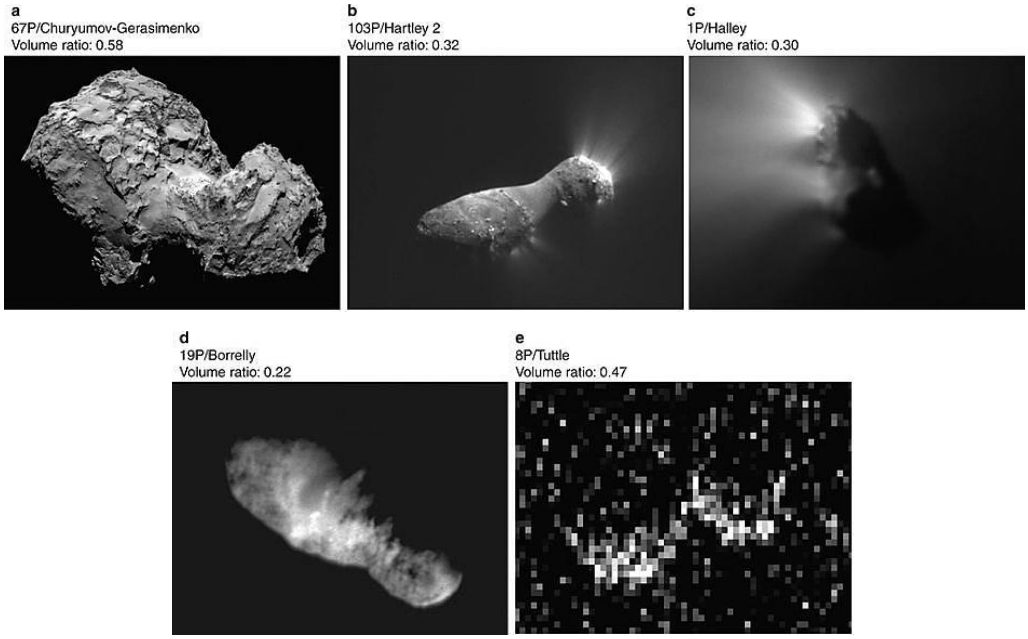

Fig. 19 Bi-lobed shapes and volume ratios of comet *a)* 67P/Churyumov-Gerasimenko *b)* 103P/Hartley 2 *c)* 1P/Halley *d)* 19P/Borrelly and *e)* 8P/Tuttle .

Solar System, before their low-velocity collision and aggregation (Massironi et al., 2015).

These considerations can be eventually extended to others comets as well, since possible stratifications are also present on the cometary nuclei of 9P/Tempel 1 and 81P/Wild 2 and many others show bi-lobed shapes as 1P/Halley, 8P/Tuttle, 19P/Borrelly and 103P/Hartley 2 (Fig. 19). This last observation, therefore, suggests that the final stage of a cometary nucleus formation can often involve the merging of two similarly-sized cometesimals (Davidsson et al., 2016).

The total volume, estimated using the shape model obtained from the OSIRIS instrument's (Optical, Spectroscopic and Infrared Remote Imaging System) images, is of about 18.7±1.2 km^3 (Preusker et al., 2015) and when combined with the total mass, estimated by the RSI instrument (Radio Science Investigation) and corresponding to $9.982\pm0.003x10^{12}$ kg (Pätzold et al., 2016), allowed to determine a mean density of about 0.535± g/cm^3 (Preusker et al., 2015), indicating a high porosity.

The CONSERT instrument (Comet Nucleus Sounding Experiment by Radio wave Transmission), instead, on the base of the propagation delays, allowed to determine a porosity of 75-85%, depending on the dust-to-ice mass ratio considered (Kofman et al., 2015). This value is consistent with a composition estimated on the basis of the elemental abundances of the carbonaceous chondrites and made up by 25% of sulfides and metals, 42% of rocks and organic materials and by 32% of ice. To obtain this composition it was assumed that all the atoms of hydrogen would be used to form water molecules, consuming thus half the oxygen atoms. The remaining atoms of oxygen, instead, would combine with magnesium, silicon, aluminium, calcium and sodium to form silicates. The carbon and nitrogen atoms would form the organic compounds, while iron, nickel and silicon would form metals and sulfides (Davidsson et al., 2016).

Further analyses highlighted that the dielectric constant decreases of about 25% within 100 m in depth: this can be explained as an increase of about 15% in porosity with depth and/or as a decrease of the dust-to-ice mass ratio from the superficial value of 4 to 0.1 (Ciarletti et al., 2015). In either case, the superficial density is higher than a hundred meters below.

The whole cometary nucleus of 67P has been divided in 26 physiographic regions based on morphological and/or topographical diversities and named after the deities of the Egyptian pantheon (in particular goddesses for the head and gods for the body of the comet) (Fig. 20).

The surface of the nucleus presents substantial morphological differences and can be classified into three main categories: consolidated materials, non-consolidated materials and large-scale depressions (El-Maarry et al., 2015; El-Maarry et al., 2016; Thomas et al., 2015).

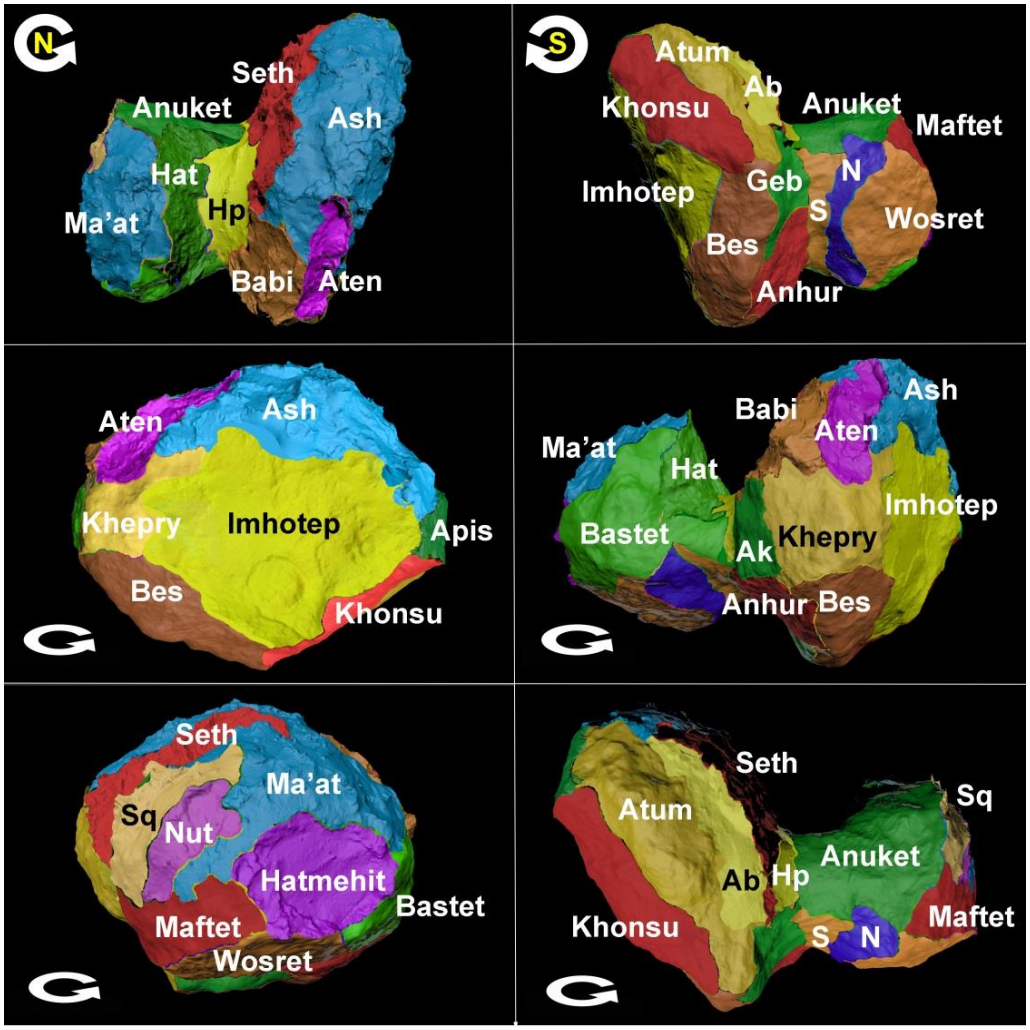

Fig. 20 All the defined regions of comet 67P in the northern and southern hemispheres with polar viewing angles (*two upper panels*) and equatorial projections with shifts of 90° (*four panels below*); the acronyms correspond to Hapi (Hp), Hathor (Hat), Sobek (S), Neith (N), Aker (Ak) and Serqet (Sq) regions (El-Maarry et al., 2016 appendix).

The term consolidated materials refers to regions that appear rocky and are cohesive enough to display sets of aligned linear features and fractures, but also refers to brittle/weakly consolidated regions that show a high concentration of circular pits and mass-wasting deposits along with fracturing and collapses (e.g. Seth) (Fig. 21). Consolidated regions are the most common on both lobes and can be fully exposed (e.g. Wosret) (Fig. 21), partially buried by dust materials (e.g. Bastet) or can enclose smooth terrains (e.g. Khepry) (Fig. 21).

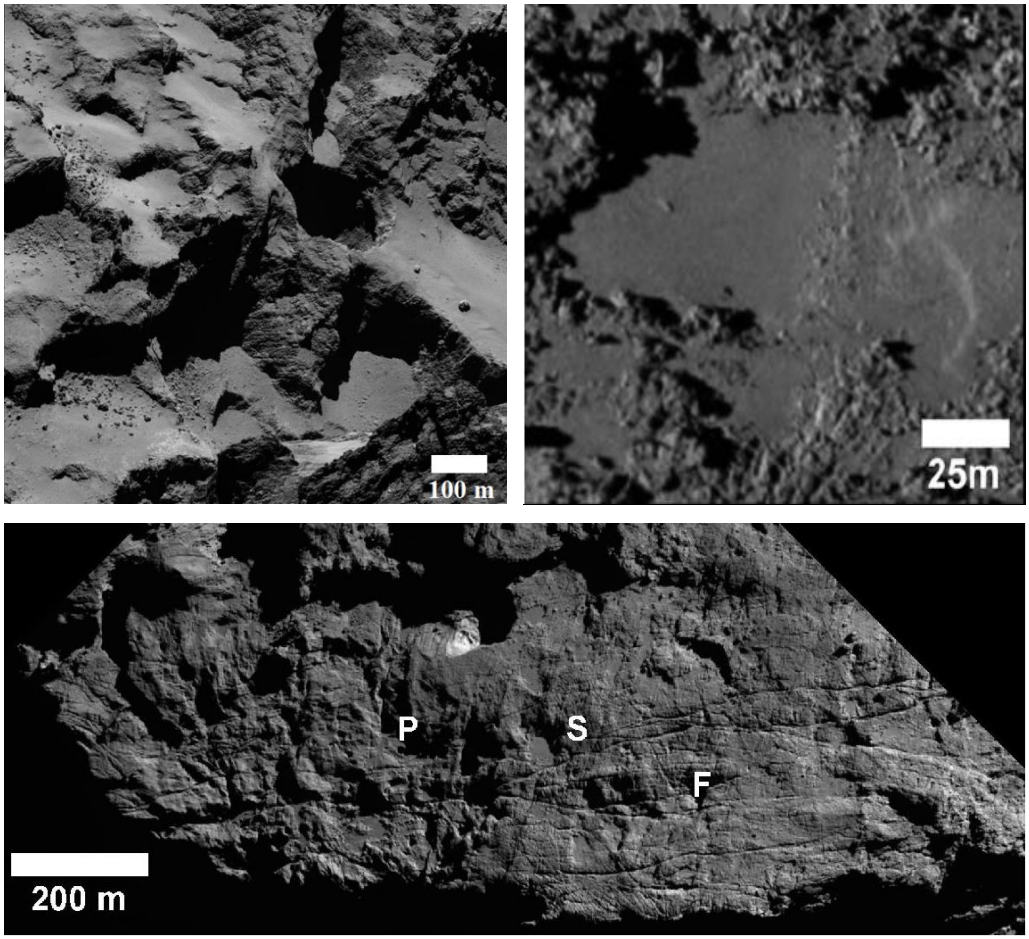

Fig. 21 Circular pit chain and mass-wasting deposits in the Seth region (*upper panel on the left*), smooth patch enclosed by consolidated terrains in the Khepry region (*upper panel on the right*) and fully exposed consolidated terrain in the Wosret region with pitted terrains (P), fractured terrains (F) and smooth terrains (S) filling pits (*panel below*) (El-Maarry et al., 2015; El-Maarry et al., 2016).

The latter refer to regions covered with extremely smooth deposits composed of non-consolidated materials, which are thick enough to mask the underlying units and that somewhere gives the impression to be layered (e.g. Imhotep) (Fig. 22). Together with the smooth terrains, the term non-consolidated materials refers also to dust-covered regions that show signs of wide-spread mobilization, such as rocks with wind tails, ripples and dunes-like structures, and where non-cohesive materials are thin enough to reveal the large-scale structures of the substrate (e.g. Ma'at) (Fig. 22). The term large-scale depressions, finally, refers to three irregular-shaped depression structure (i.e. Aten, Nut, Hatmehit) (Fig. 22) filled with mass-wasting or talus-like

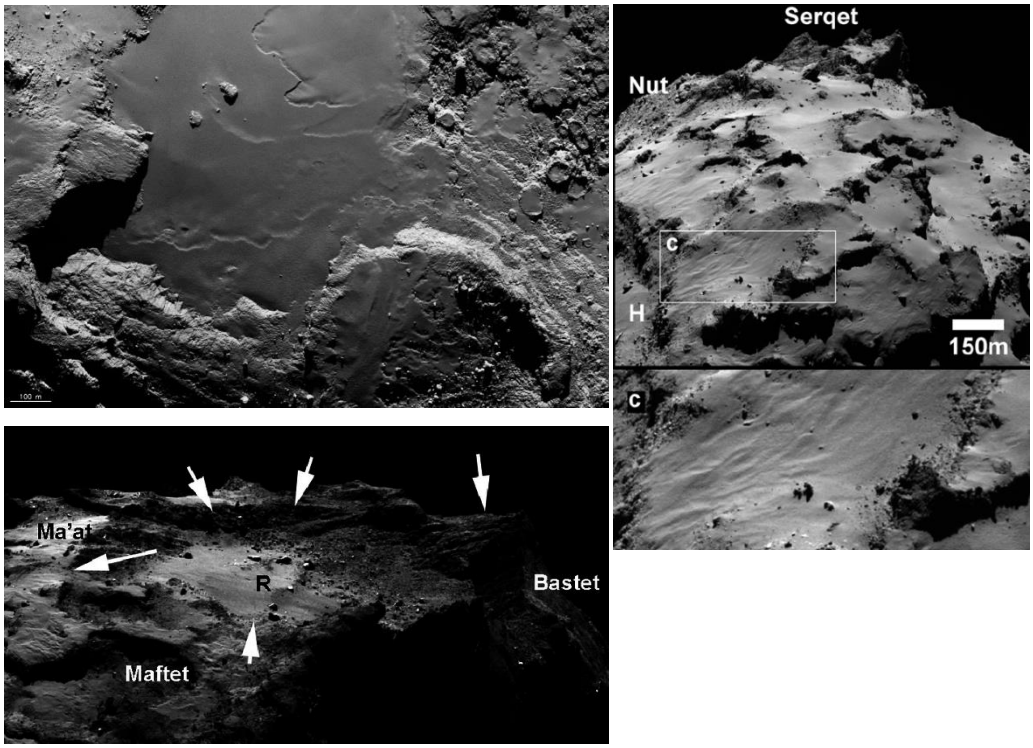

Fig. 22 Smooth terrain in the Imhotep region with layering (*upper panel on the left*), dust-covered terrain in the Ma'at region with wide-spread mobilization around the Hatmehit depression (H) and ripple-like features (*on the right*) and the Hatmehit region with the rims of the depression highlighted by the arrows, its smooth interior and talus-like debris toward the Bastet region and a curvilinear ridge (R) that crosses the depression (*bottom panel on the left*) (El- Maarry et al., 2015; Thomas et al., 2015).

deposits that may represent locations of massive outburst activity or other endogenic processes.

In general, the southern hemisphere of 67P, compared to the northern one, lacks of wide-spread smooth terrains, dust-covered regions and large depressions. Therefore it is noticeable the decrease of textural diversity in the southern hemisphere, where the regional dominating features are fractured consolidated terrains and areas exhibiting talus deposits and boulder fields. Moreover, in spite of the presence of pits, cliffs and their related alcoves, the southern hemisphere appears flattened and topographically less dynamic with respect to the northern hemisphere, and probably it may be due to higher insolation rates during its intense, even if short, summer which closely occurs with the perihelion passage (El-Maarry et al., 2016).

The overall morphology of comet 67P/Churyumov-Gerasimenko may consequently result in heterogeneities within the nucleus both in terms of physical and mechanical properties, such as porosity and strength.

However, it should be borne in mind that the two lobes are strictly similar in terms of composition and surface structures and, especially, that they both show a deep onion-like stratification.

The structural evolution of the cometary nucleus of 67P, pursued through the accretional and collisional processes within the solar nebula and protoplanetary disk and the successive processes of erosion and sublimation, led over time to the formation of an intricate system of terraces and cliffs, hogbacks, cuestas and mesas on which it is possible to see the morphological evidences of the stratification.

The sets of fractures are very common on the cometary nuclei (Fig. 23) and can be generated by collisional events or thermal fatigue processes or induced by rotational torques. Their origin can be inferred from their orientation, localization and geometrical characteristics.

The thermal fatigue, for example, caused by the huge temperature ranges experienced by the cometary nucleus over daily and orbital time scale, can lead to the formation of pervasive polygonal fractures that, along with the sublimation processes, may provoke the detachment and isolation of meter-sized blocks which constitute surfaces characterized by globular shapes forming goose-bumps textures (Sierks et al., 2015). These bumps exhibit

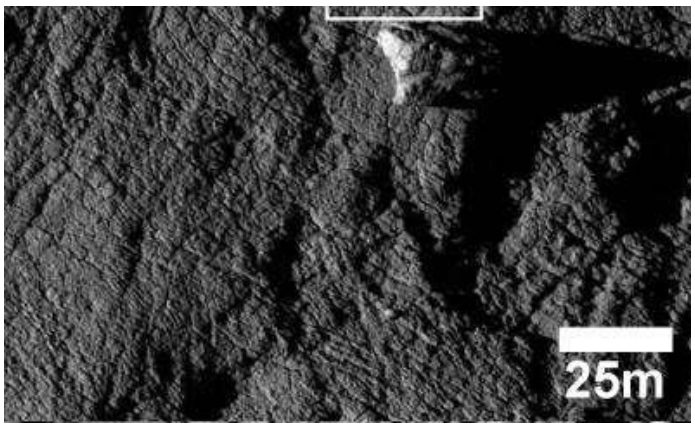

Fig. 23 Polygonal fractures on 67P due to thermal fatigue processes.

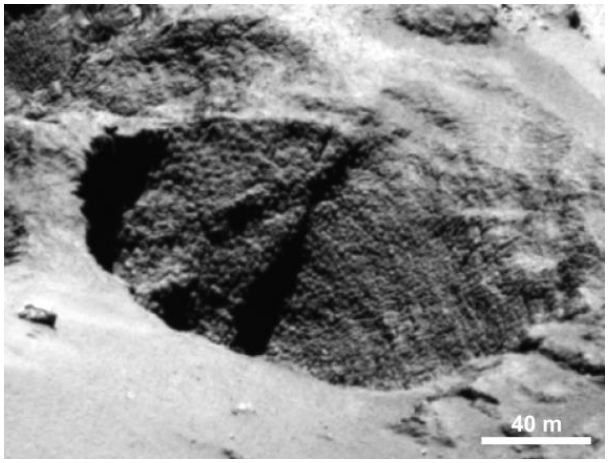

Fig. 24 Goosebumps texture in an active pit in the Seth region (Sierks et al., 2015).

rounded shapes and characteristic scale ranging from 1 to 5 meters and can be find in several places on the nucleus (Davidsson et al., 2016) (Fig. 24).

The rotational torques, instead, may induce the development of internal stress that, as in the neck region (i.e. Hapi) that divide the two lobes of comet 67P, can lead to the opening of tensional longitudinal fractures long even a hundred meters (Fig. 25). Finally, the collisional events of accretion or impact may generate systems of radial and planar fractures respect to the impact point. The latter would be the case of the fractures that affect the cliff of Hathor, a wall of 900 m located at the contact between the neck and the smaller lobe of comet 67P (Fig. 26).

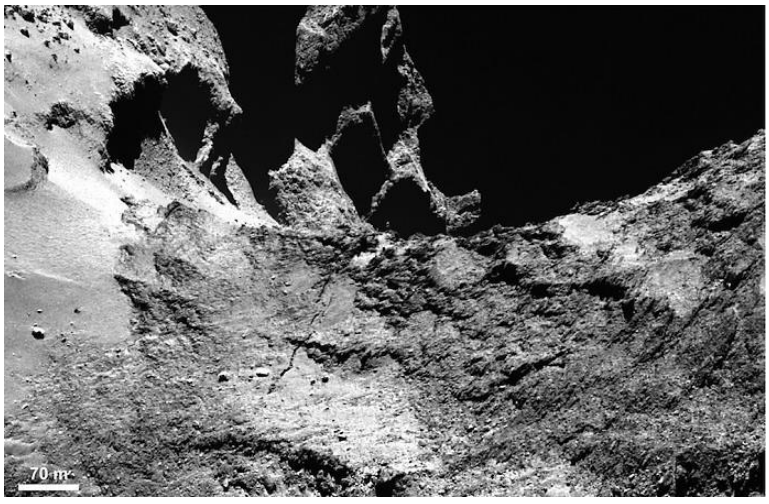

Fig. 25 Fracture extending in the Hapi and Anuket regions.

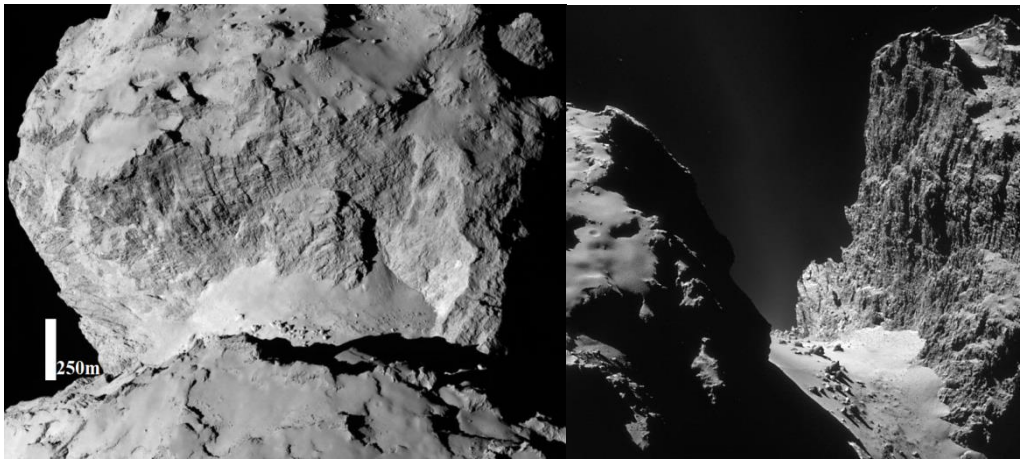

Fig. 26 Hathor's cliff with its fractures due to collisional events (Sierks et al., 2015; Thomas et al., 2015).

Together with the primary structures, that show the primordial genesis of the comet, the morphology of the cometary nucleus is also characterized by erosive features and their deposits, that prove the evolutionary history of the planetary body.

The erosion of a cometary body is principally driven by the sublimation and degassing processes. However, as previously introduced (See ch. 1.4), the cometary activity cannot affect all the nucleus, depending on the illumination conditions, the proximity of the perihelion and the general morphology, and can also reflect distribution variations of the refractory covering or inner compositional heterogeneities. If the cometary activity is present, it can lead to selective erosion and sublimation mechanisms and to gravitational phenomena.

The presence of inner compositional heterogeneities, for example, can lead to the sublimation of subsurface layers (See ch. 1.5) and the generation of internal voids, whose expansion may cause collapses of the cavity roofs to form pits. The pits become broader due to retrogressive erosion of their walls, which may also collapse leading to the formation of semi-circular terraces. This lead to the exposure of new fresh walls, on which sublimation focuses generating jets (Fig. 27).

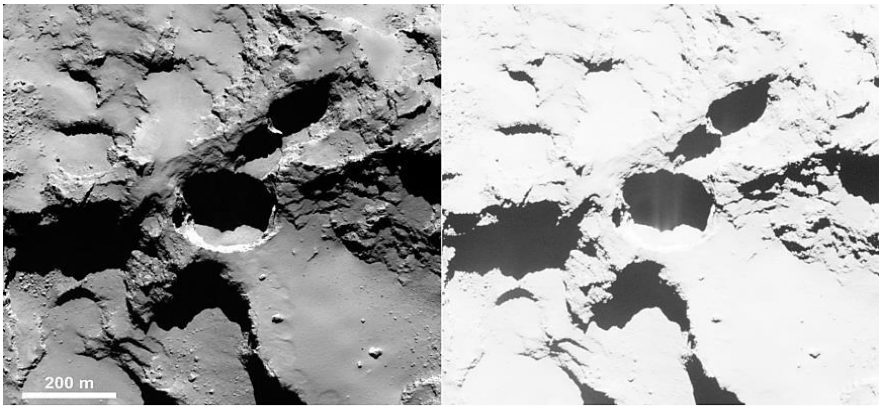

Fig. 27 Active pit in the Seth region: enhancing the contrast it is possible to see the fine structures in the shadow of the pit interpreted as jets (Sierks et al., 2015).

Pits with similar morphologies have been observed also on comets 9P/Tempel 1 and 81P/Wild 2, where they were interpreted as activity-related depressions. The pits on the nucleus of 67P, when active, tend to have a depth/diameter ratio close to 1, while the inactive ones are much shallower, probably due to the filling of fine air-fall materials and landslide deposits (Sierks et al., 2015).

Opposite to the pits' depressions, there are mesas and cuestas morphologies that are generally described as a result of slope retreat driven by sublimation on compositionally heterogeneous strata. The scarps underlying mesas and terraces are strictly related to gravitational phenomenon and therefore it is very common the formation of rock-fall deposits (Fig. 28).

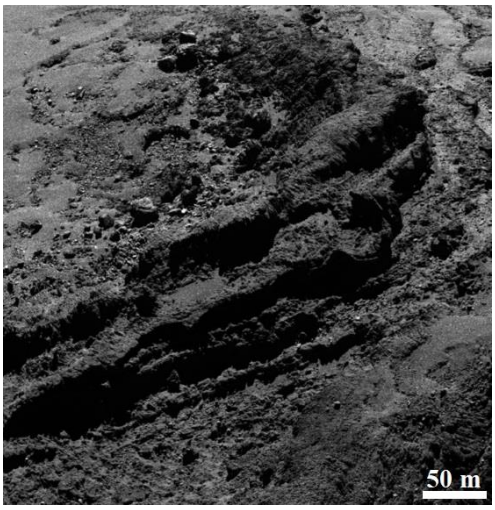

Fig. 28 Mesa morphology with its stratification and rock-fall deposits.

Being equal in refractory dust cover, the sublimation mechanisms appear to be widespread on large areas and not concentrated solely along pit walls and cliff. Some areas, indeed, are interested by the cyclical sublimation processes in function of the illumination conditions over the local day. In this case the activity is only partially connected to the exposure of ices and mainly depends on a sort of daily water cycle. During the day, when the surface is illuminated, water ice sublimates from the uppermost layers, but when the surface goes into shadow, during the local night, a temperature inversion takes place between the surface and the inner subsurface due to the thermal inertia of the material. Water vapor, produced by the subsurface sublimation of the now warmer inner layers, percolates through fractures and pores and crystalize as water ice close to the surface until a new cycle of solar illumination leads to its sublimation (De Sanctis et al., 2015) (Fig. 29). The repeat of this process may have led to the accumulation of great quantities of ice within the first tens of meter in depth. Anyway, this process does not substitute the primordial layered material that constitute the cometary nucleus but it only affects its rheological properties.

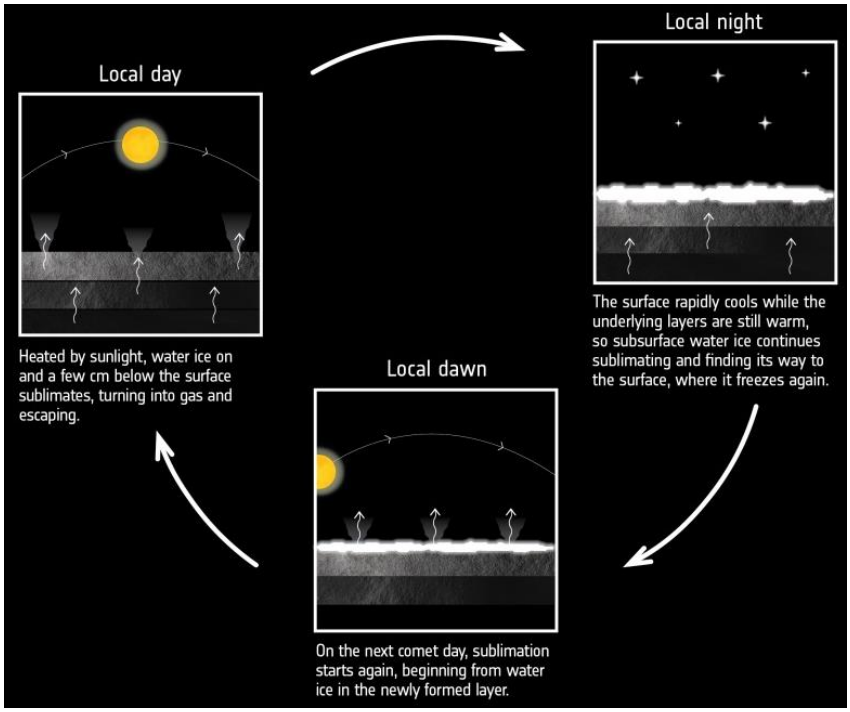

Fig. 29 Water cycle on comet 67P.

Additional morphological forms related to the sublimation processes are the aeolian-like structures, such as ripples, dunes and rocks with wind tails, formed on areas characterized by the presence of dust-covered terrains, that support the idea of localized gas-driven transport (Thomas et al., 2015). However, the gas expansion must overcome the gravitational force and the grains cohesion to initiate saltation, and this is prevented by the rapid decrease of the pressure profile. Another process is the air-fall splash effect due to the fallout of particles previously lifted by sublimation processes that, failing to escape from the nucleus, re-impacted on the surface with enough energy to exceed the particles' cohesion and to cause their motion.

The spectrophotometric properties of the cometary nucleus of 67P derived from the OSIRIS observations allowed to study the heterogeneities of the nucleus both in terms of albedo and composition (Fornasier et al., 2015).

In general, the nucleus has similar spectrophotometric properties in the NUV-VIS-NIR wavelength range to those of others bare cometary nuclei. Comet 67P shows a red spectral behavior, meaning that the reflectance increases with wavelength. Generally, no clear absorption bands are visible, except for an absorption feature at ~290 nm, that could be due to SO_2 ice, and another faint absorption feature centered between 800-900 nm, that may be associated with the Fe^{2+}-Fe^{3+} charge transfer absorption band in silicates. However, this latter interpretation and the study of the absorption features in the near-infrared regions is complicated by the enhancement of flux in the 700-750 nm region which is associated with cometary emissions in the coma, probably due to the presence of H_2O^+.

The analysis of the spectral slopes versus phase angle show a strong phase reddening for the nucleus, which is potentially attributed to the increased contribution of the multiple scattering at large phase angles and to surface roughness effects.

The spectral slope is anticorrelated with the reflectance, therefore higher spectral slope values correspond to redder surfaces and thus to darker regions, while bluer spectral slopes characterize brighter regions as Hapi,

which is both the brightest, bluest and the most active surface on the comet at large heliocentric distances (>3 AU), due to the higher abundance of water ice which is often cast in shadow (Fig. 30).

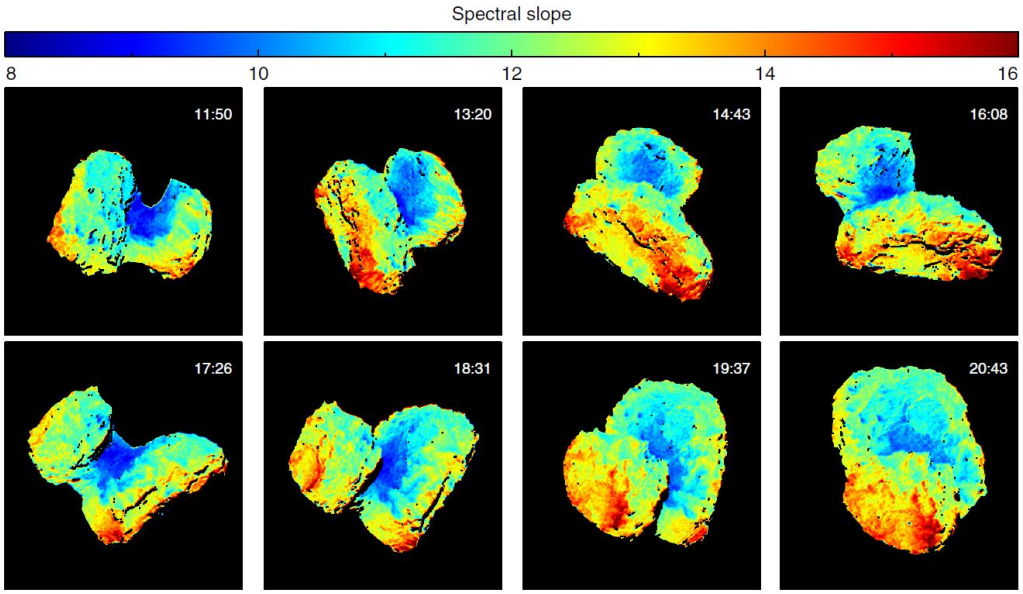

Fig. 30 Spectral slope of pre-perihelion images computed in the 535-882 nm range, after normalization at 535 nm, and it is in %/(100 nm) (Fornasier et al., 2015).

The overall cometary nucleus of 67P/Churyumov-Gerasimenko has a surface dark in absolute terms with an estimated geometric albedo of 6.5±0.2 at 649 nm, meaning that it is brighter but still similar to that found for comets 9P/Tempel 1 and 81P/Wild 2. Across the nucleus, the albedo shows local variations: in particular, Hapi shows local albedo variations up to +16%, while regions as Ash and Seth are about 9% darker.

Computing the spectral slope together with local spectrophotometry it is possible to identify three distinct groups of regions characterized by low (i.e. blue), medium and high (i.e. red) spectral slopes. The groups' spectral slope properties highlight that they are not correlated to particular morphologies and not representative of vertical diversity in the nucleus composition.

The VIRTIS instrument (Visible and InfraRed Thermal Imaging Spectrometer) results indicate a global surface composition dominated by dehydrated and organic-rich refractory materials (Capaccioni et al., 2015), even

though several local bright spots were identified in the OSIRIS images and interpreted as exposures of water ice (Fornasier et al., 2016).

Approaching the perihelion, reached the on 13 August 2015, the nucleus of 67P became relatively bluer, with a decrease in the spectral slope up to -30% and considerable diurnal color variations, and the phase reddening decreased by a factor of two. This suggests that the increasing level of activity removed the overlying refractory mantling material leading to the exposure of the underlying ice-rich layers and therefore to bluer nucleus' colors (Fornasier et al., 2016).

The presence of water ice was identified only in active regions or on newly exposed fresh surfaces. With the analysis of the ROSINA instrument (Rosetta Orbiter Spectrometer for Ion and Neutral Analysis), moreover, it was possible to observe daily and latitudinal compositional variations with local dominance of extremely volatile materials with respect to the general dominance of water ice, which is also present in amounts three times greater in the northern hemisphere compared to the southern one (Fulle et al., 2016).

3.1 Regions of interest

In this work we decided to study the Wosret and Bastet regions (El-Maarry et al., 2016), both located on the small lobe, the head, of the comet 67P/Churyumov-Gerasimenko. On the basis of the three dimensional ellipsoid-based model (Penasa et al., accepted), which defines the structural level of any point on the surface as a distance from the structural centre of each lobe, these regions, represent a geological section on the onion-like stratification of the comet (Massironi et al., 2015), with the outermost layers located in Bastet and in the part of Wosret toward the Maftet region and the part of Wosret toward Neith corresponding to the innermost layers (Fig. 31).

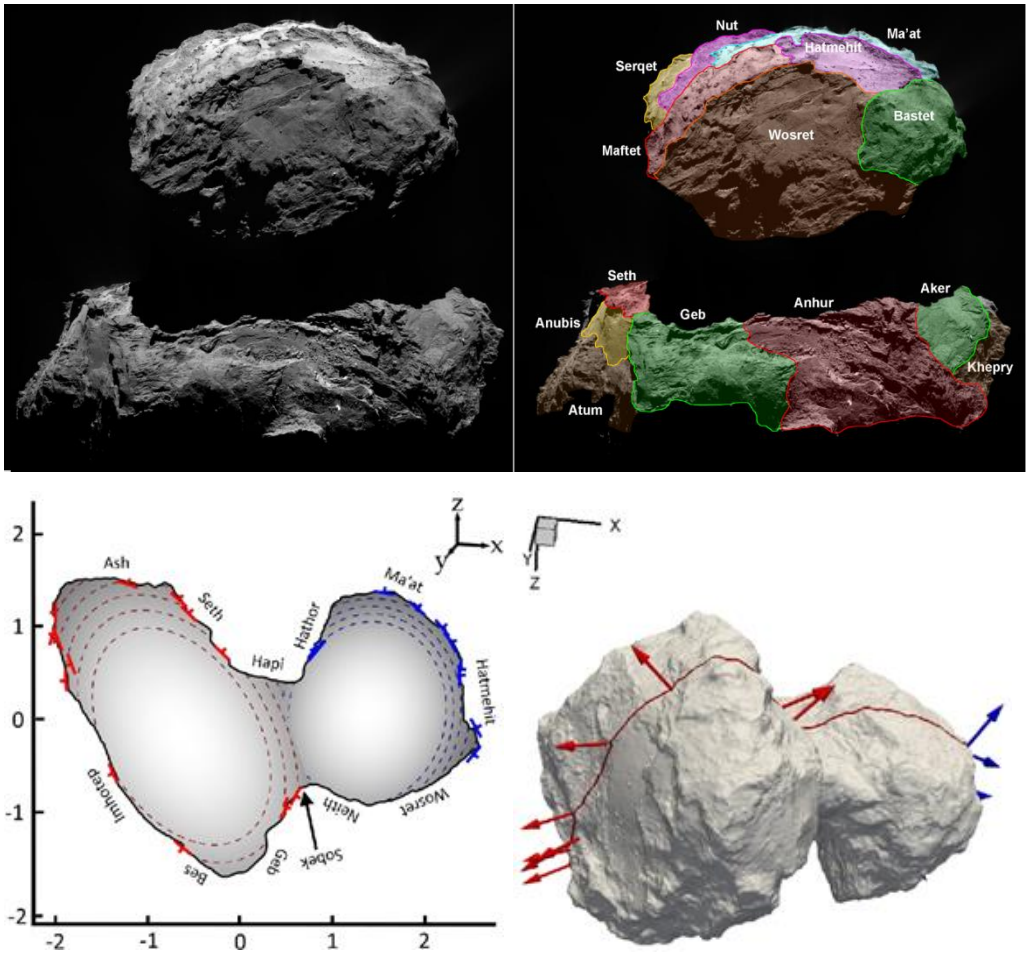

Fig. 31 View of the southern hemisphere of comet 67P with the Wosret and Bastet regions (*upper panels*) and hypothetical geological section of comet 67P with the local orientation of the layers (blue and red symbols respectively for head and body) and the interpretation of the subsurfaces (dashed lines) (*bottom panel on the left*) and the intersection of the section plane with the topography, where the arrows indicate the normal vectors to the inferred layers (*bottom panel on the right*) (El-Maarry et al., 2016; Lee et al., 2016).

Approximately, the entire southern hemisphere face of the smaller lobe is included in the Wosret region, which appears to be topographically flat, with some major changes of relief near the boundary with the Maftet and Hatmehit regions, and characterized by outcropping consolidated terrains with both heavily fractured and pitted areas. Close to the Hatmehit depression, indeed, pits have been identified with diameters ranging between 45-100 m (Fig. 32). Toward the Maftet region various almost parallel lineaments form three bands of layered material with spaces of a hundred meters from each other. Toward the neck region (i.e. Neith) the rough surface is marked by

several fractures reaching 300 m in length (Fig. 32) and crosscutted by smaller ones forming polygonal fracture patterns. On one side Wosret borders the Bastet region: their boundary is characterized by a scarp with debris and boulders (Fig. 32). The Bastet region is a rough consolidated region that straddles the northern and southern hemispheres. Overall, Bastet presents preferred alignment of long lineaments mostly located in the central northern hemisphere part of the region (Fig. 32), while the southern hemisphere part is more fractured and darker in tone, probably due to the lack of thick lighter-toned dust coatings (Fig. 32) (El-Maarry et al., 2015; El-Maarry et al., 2016; Lee et al., 2016).

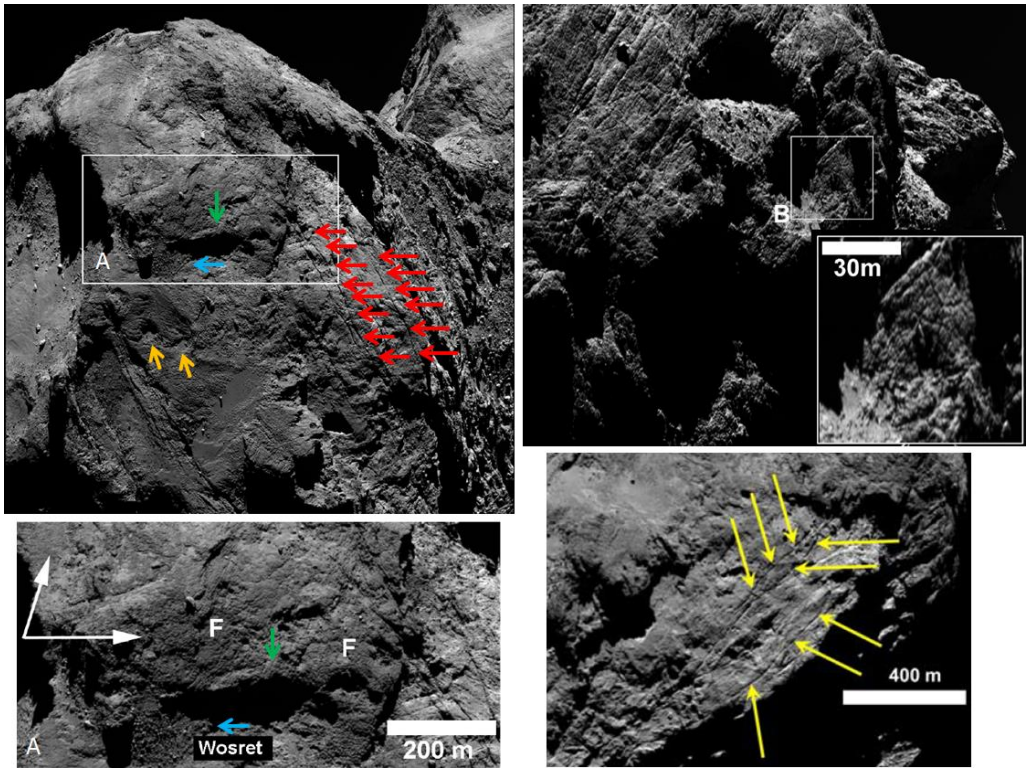

Fig. 32 Image showing the Bastet and Wosret regions with the presence of pits (ochre arrows) and fractures (red arrows) and highlighting the presence of a scarp (green arrow) and debris with boulders (blue arrow) at the boundary between the two regions (*upper panel on the left*). A zoom of the Bastet-Wosret boundary that shows the difference in tone (white arrows) between the northern portion of Bastet (brighter) and its southern part (darker) (*bottom panel on the left*). A zoom of the fractures (yellow arrows) present in the part of Wosret toward the neck region (*bottom panel on the right*). Image showing the fracturing pervading the northern portion of the Bastet region (*upper panel on the right*) (El-Maarry et al., 2015; El-Maarry et al., 2016; Lee et al., 2016).

3.2 Aim of the thesis

The principal aim of this thesis is to give an advance in the study of small bodies, and in particular comets, through the analysis of high-resolution close-up images acquired by the spacecraft Rosetta during the escorting of the comet 67P/Churyumov-Gerasimenko.

Since the peculiar bi-lobed shape of the comet 67P is considered to be the result of a low-velocity collision between two distinct bodies sharing a similar onion-like stratification (Massironi et al., 2015), the aim of this thesis is to study some regions on the smaller lobe (head) of the comet (El-Maarry et al., 2015; El-Maarry et al., 2016) to identify at least two different envelopes and to verify if the stratification defined by the ellipsoid-based model (Penasa et al., accepted) presents spectrophotometric variations.

Once and if identified, it would be possible to understand on what basis the shells difference themselves, both in terms of compositional or textural variations, and what this could tell us about the evolution of the comet 67P during its formation and development.

4. Methodologies

4.1 Data

The images used for this work were acquired with the OSIRIS imaging system (Optical, Spectroscopic and Infrared Remote Imaging System), which consists of two independent camera systems sharing common electronics (Fig. 33). The Narrow Angle Camera (NAC) was designed to produce high spatial resolution images of the nucleus of the comet (up to 2 cm/px from one kilometer away). The Wide Angle Camera (WAC), instead, was optimized for high resolution panoramic images of the gas and dust particles surrounding the cometary nucleus of the comet. Each camera was equipped with filter wheels (12 for NAC, 14 for WAC) which allowed the acquisition of images for various scientific purposes, in an overall wavelength range between 250 and 1000 nm (Keller et al., 2007) (Table 3).

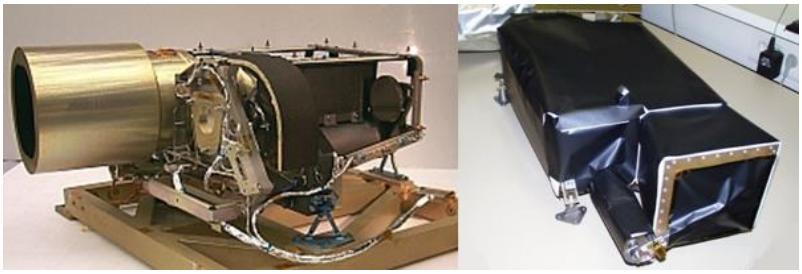

Fig. 33 NAC (*on the left*) and WAC (*on the right*) OSIRIS cameras.

Table 3 NAC-OSIRIS wheel filters.

NAC filter	Name	Wavelength (nm)
F15	Far-UV	269.3
F16	Near-UV	360.0
F24/F84	Blue / Neutral_Blue	480.7
F23/F83	Green / Neutral_Green	535.7
F32	Neutral	640.0
F22/F82	Orange / Neutral_Orange	649.2
F27	Hydra	701.2
F28/F88	Red / Neutral_Red	743.7
F51	Ortho	805.3
F41	Near-IR	882.1
F61	Fe_2O_3	931.9
F71	IR	989.3

We searched in the OSIRIS images archive (website address: https://planetgate.mps.mpg.de:8114/) as many sequences of images as possible framing the physiographic regions selected for this work.

The images were acquired by the Narrow Angle Camera. The selected sequences cover the maximum number of available filters for the chosen regions, are converted in radiance factor (I/F) and have similar spatial resolution and phase angles lower than 90° (Table 4).

Table 4 List of the selected images.

Set	**Date**	**Time**	**Filters**	α_{F27} [°]	Δ_{F27} [km]	Res_{F27} [m/px]
A	2016-02-10	07:05-07:07	15-22-23-24-16-27-28-41-51-61-71	65.7610	50.8259	0.95
AB	2016-01-27	21:22-21:24	22-23-24-27-28-41-71-61-16	62.2409	69.3909	1.3

The chosen sequences were named set A and set AB and were made up respectively of 11 and 9 images (Fig. 34).

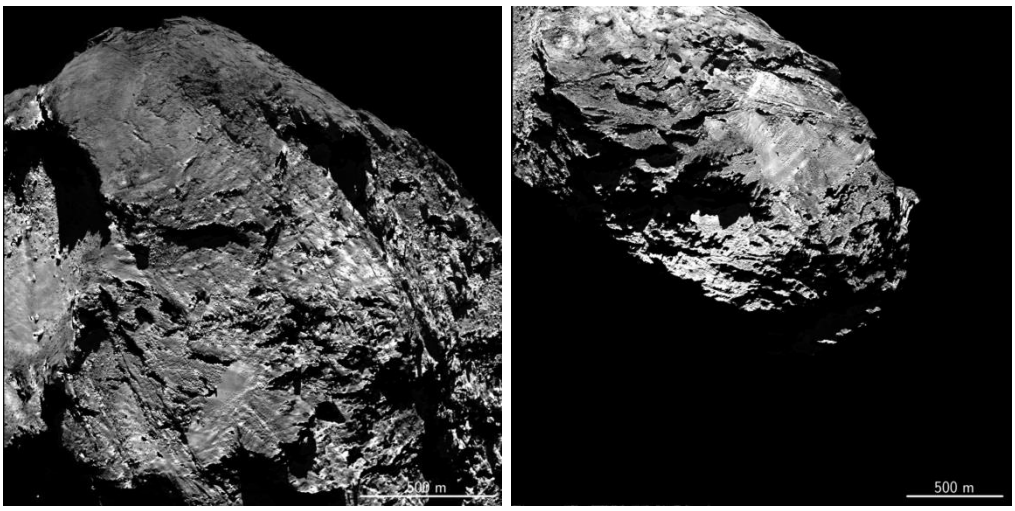

Fig. 34 Set A (*on the left*) and AB (*on the right*) with F27 (701 nm) central filter.

The shape model by Preusker et al. (2015), the NAIF-SPICE data by NASA and the ellipsoid-based model by Penasa et al (accepted) were used to perform our analyses.

The shape model (i.e. topographic model) of the comet is a mathematic model that defines the geometry of the comet 67P in every point in three-dimensional coordinates. It was obtained using the OSIRIS NAC image data along with stereo-photogrammetric methods to reconstruct the irregular shape of the cometary nucleus.

The NASA's Navigation and Ancillary Information Facility (NAIF) is an observation geometry information system focused on Solar System geometry, named "SPICE", that assists scientists and engineers in interpreting the scientific observations from space-based instruments onboard the spacecrafts. Using these data it is possible to compute derived observation geometry such as altitude, latitude/longitude and lighting angles.

The three dimensional onion-shell ellipsoidal model (Penasa et al., accepted), finally, derived measuring the orientation of terraces on the cometary nucleus of 67P, can be used to evaluate the structural level of any point on the surface as a distance from the structural centre of each lobe.

4.2 Cube creation and photometric corrections

The images, for each sequence, were reorganised according to the filter's wavelengths and, in order to stack them, several ground control points (GCPs) were positioned image to image with Exelis Envi Classic, adopting as reference image for each set the F27 (701 nm), chosen for its centrality both in terms of acquisition times and wavelength.

For every pair of images at least 40 GCPs were selected, homogeneously located between pixels with a good greylevel contrast and trying to minimize the route mean square errors (RMS) due to the positioning of the points (Fig. 35).

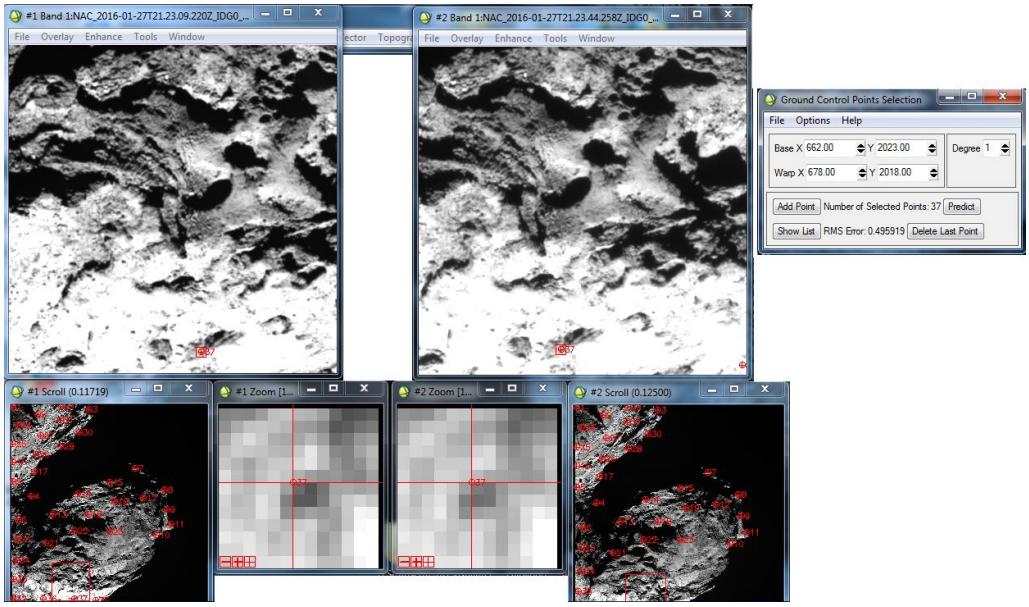

Fig. 35 GCPs positioning with Exelis Envi Classic.

The images of each set were successively aligned with the programming software Exelis IDL. Using the software every image, excluding the F27 adopted as reference, was warped using the WARP_TRI function, a linear interpolation method.

Therefore two multispectral cubes were constructed, where two dimensions were defined by the spatial information (2048 x 2048 px) and the third dimension was defined by the spectral information, namely the reflectance referred to its wavelength.

A photometric correction was then applied to the cubes in order to delete the effects due to the different illumination and topographic conditions and thus to allow the distinction of the physical characteristic of the material from the mere geometric conditions. Hence, it was necessary to use a photometric model to understand how and how much light was reflected by the surface.

To obtain the radiance factor values photometrically corrected we decided to apply the Akimov correction, a function that does not require additional parameters (e.g. as the Hapke function), and it is thus less vulnerable to errors and stretches (Akimov L.A., 1976; Akimov L.A., 1988; Shkuratov et

al., 1994; Shkuratov et al., 2003). This correction was judged suitable for the study of the comet 67P/Churyumov-Gerasimenko given its low albedo and the extreme roughness of its surface (La Forgia et al., 2015; Shkuratov et al., 2011).

To apply the function was necessary to own the shape model (i.e. topographic model) of the comet (Preusker et al., 2015). This allowed us to obtain the information pertinent the illumination conditions or, in other words, the information concerning the angles of emission *e* (between the perpendicular to the surface and the observer) and incidence *i* (between the Sun and the perpendicular to the surface) and the phase angle α (between the lines of sight and solar incidence) (Fig.36).

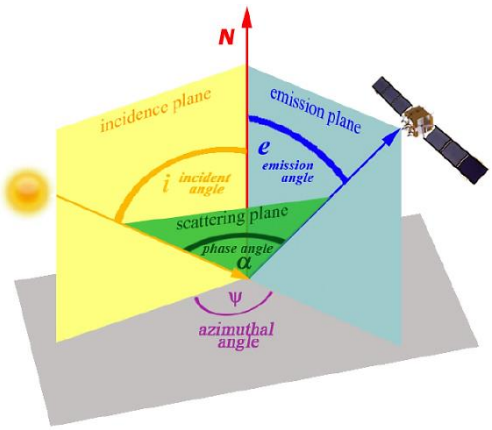

Fig. 36 Angles and planes scattering geometry.

With the shape model and the information of the NAIF-SPICE data it was possible to create a synthetic image, which reproduced pixel by pixel the same illumination and acquisition conditions of the original image and that allowed to extract the maps concerning the emission, incidence and phase angles at the moment of the image acquisition.

However, the synthetic image presented some differences with respect to the original one due to faint imprecisions of the SPICE data (e.g. geometric information), therefore it was necessary to perform a second operation of positioning of GPCs, warping and stacking of the synthetic and original images.

This was followed by the warping of the three maps concerning the angles *i*, *e* and α. We decided to remove all the data with *e* and *i* greater than 80°, to delete less informative data. Then we calculated the cosine of the emission and incidence angles and the sine and cosine of the phase angle, from which depend the photometric parameters β and γ calculated as a result. Knowing these parameters was possible to determine the Akimov's disk function *D*. Applying this function we extracted pixel by pixel the radiance factor photometrically corrected (Fig. 37) and we omitted from the analysis all the pixel outside the cometary surface.

$$\cos i = \cos\beta\cos(\alpha-\gamma)$$

$$\cos e = \cos\beta\cos\gamma$$

$$D(\alpha,\beta,\gamma) = \cos\frac{\alpha}{2}\cos\left(\frac{\pi}{\pi-\alpha}\left(\gamma-\frac{\alpha}{2}\right)\right)\frac{(\cos\beta)^{\frac{\alpha}{(\pi-\alpha)}}}{\cos\gamma}$$

$$\frac{I}{F_{Acorr,\lambda}} = \frac{\frac{I}{F_{meas,\lambda}}}{D(\alpha,i,e,\lambda)}$$

Fig. 37 Formulas to calculate the Akimov's disk function and the radiance factor.

Finally, the F15 (269 nm) and F51 (805 nm) bands, not present in the cube AB were excluded from the visualization in cube A. In this way the results concerning the transformations and classifications of the corresponding cubes (See ch. 4.3) should be equivalent in terms of wavelength and be thus comparable.

4.3 Geomorphological map, identification of ROIs and image classification on the basis of the structural model

In order to perform the images classification, all the unclassifiable data by the software and the data not necessary for this work needed to be removed (i.e. excluded) from the elaboration. Therefore we proceeded, using Exelis Envi Classic, to the pre-processing of the cubes.

Given that the software is not able to classify NaN (not a number) data, namely those pixel that represent the space bottom and the cometary areas excluded during the photometric correction, to these data was attributed zero value. Successively, all the values equal to zero were masked, and thus excluded from every successive image classification, with the command "ignore value".

Since this study focuses on the smaller lobe of the comet 67P we decided to exclude from the elaboration all the areas concerning the bigger lobe. In this way it was possible to remove also the data that led to a prospective offset and to the increase of the RMS error during the stacking of the images. For each sequence thus was created a region of interest (ROI) on the bigger lobe, to which was given output value zero and was successively masked.

Finally, given that in the shadowed areas were present residual values due to faint misalignment of the filters we decided to exclude from both the cubes all the pixels with reflectance values lower than 0.002, a value that in shadowed areas results in a sudden spectral slope increase.

As last pre-processing step, just to be sure, we directly modified the header of the cubes to verify the correct exclusion of all the data with output value equal to zero from the successive elaborations.

Before proceeding with the classification, for each cube we realized a geomorphological map with Esri ArcGis, distinguishing three principal units corresponding to mass-wasting deposits, probably generated by sublimation and gravitational collapses, fine material, characterized by smooth dust coatings probably due to airfall deposition, and outcrop, meaning consolidated material of primary importance for the identification of the stratification. The result of the geomorphological mapping highlighted that our regions are mainly constituted of outcropping consolidated material with a few mass-wasting deposits, near scarps and terraces, and only a few areas of dust coating (Fig. 38). The aim of these maps was thus to help us to understand where we had to arrange the ROIs necessary for the successive classifications.

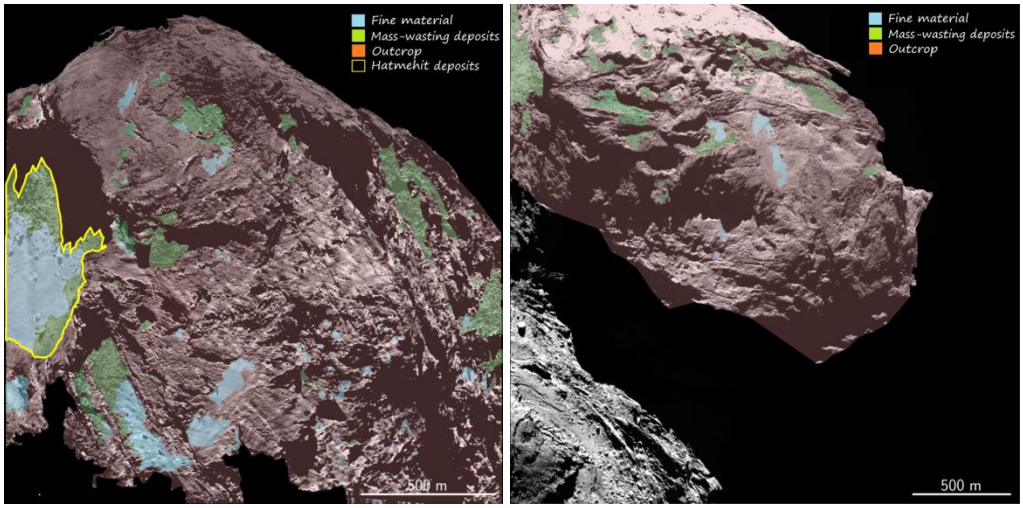

Fig. 38 Geomorphological mapping of cube A (*on the left*) and AB (*on the right*) realized using Esri ArcGis.

Using the software Exelis Envi Classic, therefore, we decided to perform unsupervised (K-Mean) and supervised classifications (Maximum Likelihood) to verify on what basis and how the software separated the pixels, taking into consideration a given number of classes and the potential training sites defined by the user.

The cubes were initially elaborated performing the unsupervised classification K-Mean, in which the software divides automatically the pixels in a fixed number of classes defined by the user and adjusts them with successive iterations.

As starting point we used two classes, which should identify the outcrop, and its related mass-wasting deposits, and the fine material. This should be possible since the latter differs from mass-wasting deposits and outcrop, because of its lack of sublimable materials (i.e. volatile content) due to the sublimation processes and the consequent development of jets that lead to airfall deposition of particles not autochthon of our regions. The result of this first classification was not particularly satisfying for both the cubes, since the fine material areas were not well identified or distributed (Fig. 39).

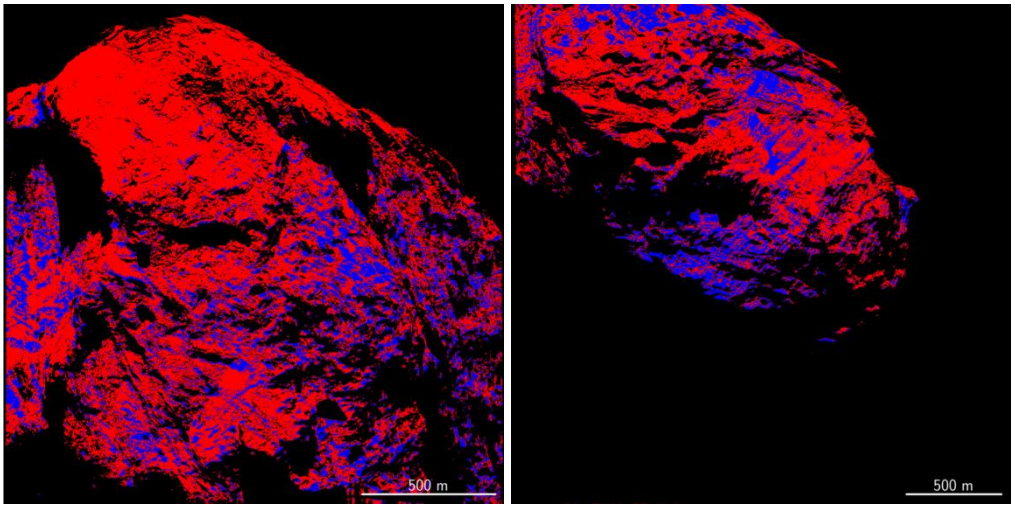

Fig. 39 K-Mean unsupervised classification of cube A (*on the left*) and AB (*on the right*) with two classes in red and blue.

The supervised classification, instead, demonstrated to be a more reliable method for the separation of the fine material from the outcrop. To proceed with this elaboration we created several regions of interest (ROIs), defined on the basis of the geomorphological maps previously realized, in areas identified as outcrop and fine material. These ROIs were created in different location to augment the range of identifying pixels of each class and to reach a quantity of pixels of at least 30 times the number of filters, this to guarantee the minimum number of pixels needed for the classification (Fig. 40).

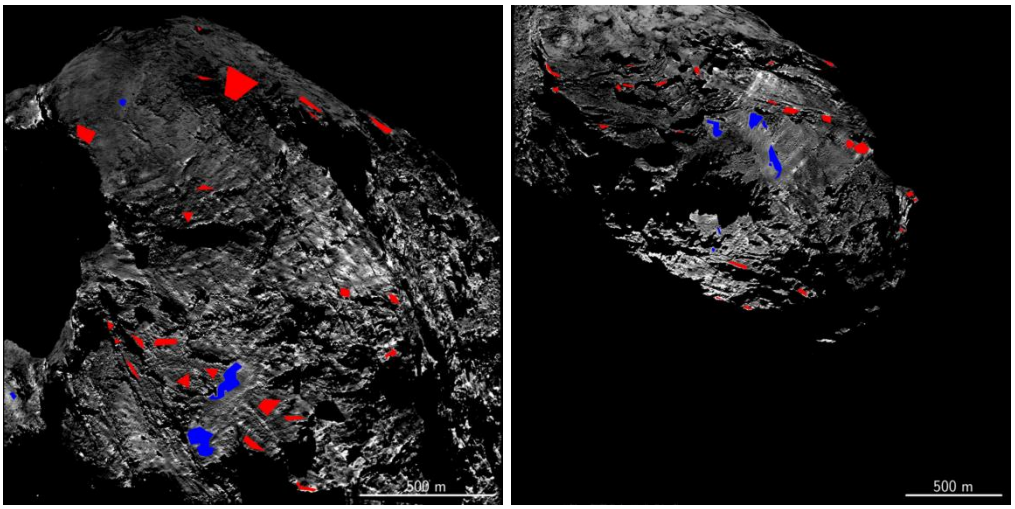

Fig. 40 ROIs selection on cube A (*on the left*) and AB (*on the right*) in areas identified as outcrop, in red, and fine material deposits, in blue.

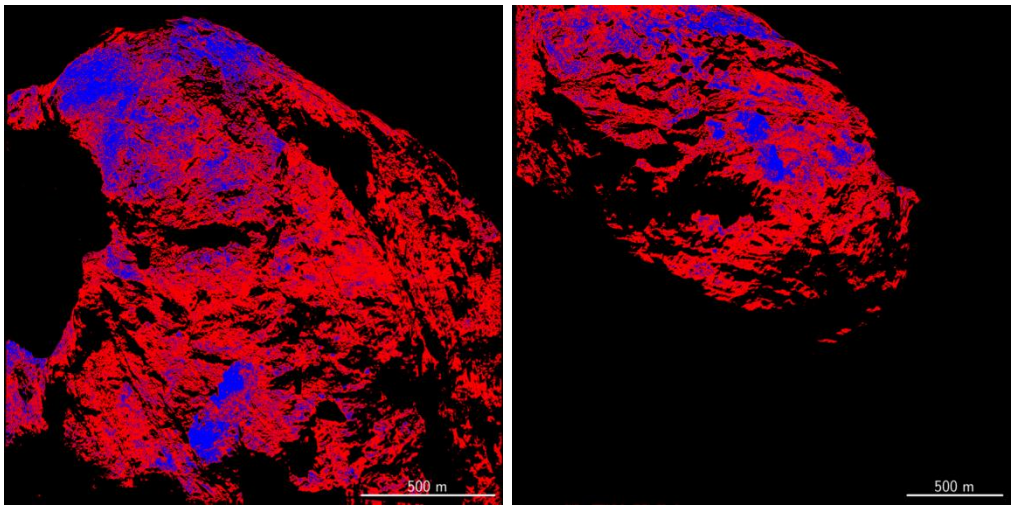

Fig. 41 Maximum Likelihood supervised classification on cube A (*on the left*) and AB (*on the right*) with outcrops and mass-wasting deposits in red and fine material deposits in blue.

The regions of interest defined were thus used to realize a supervised classification Maximum Likelihood (MLL), in which the user defines the guidelines (ROIs) that the software have to follow to distinguish the classes. The result was quite satisfactory: the class attributed to the fine material corresponded for both the cubes to the related mapped unit, including also outcropping areas where the dust coating was extremely thin (Fig. 41). Once identified, the fine material classes were converted from raster file to vector file to allow the construction of masks to be applied to the respective cube, in order to exclude the data concerning the fine material. This allowed to obtain a cube ideally made up only by outcrop and mass-wasting deposits (Fig. 42).

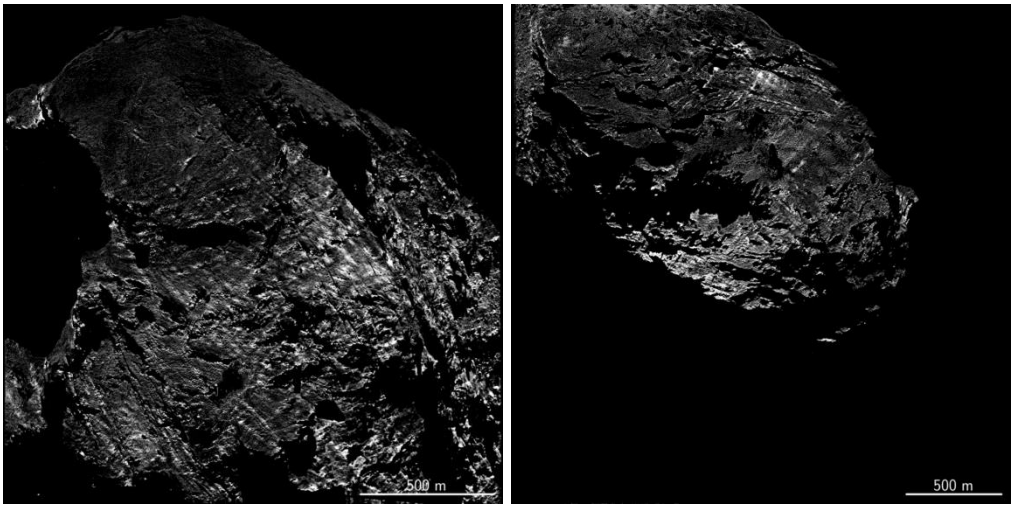

Fig. 42 Fine materials exclusion from cube A (*on the left*) and AB (*on the right*).

New ROIs were then created on the outcropping material on the basis of the elevation model (Penasa et al., accepted) attempting to identify the outer shells and the inner shells. The polygons of the ROIs corresponding to the same class were selected on the same height to maintain a certain uniformity of the datum (Fig. 43).

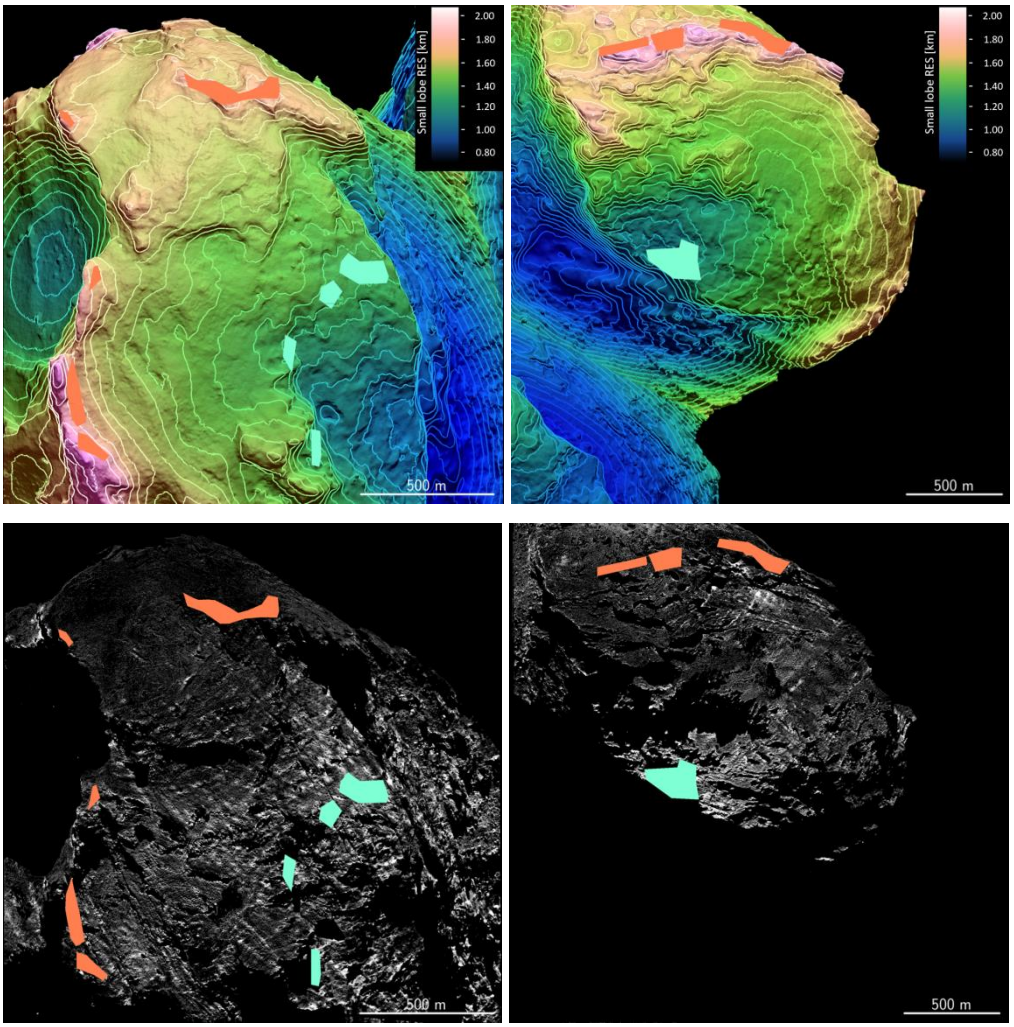

Fig. 43 ROIs selection on cube A (*panels on the left*) and AB (*panels on the right*) in areas with different elevation, high and low elevations respectively in coral and aquamarine, on the basis of the ellipsoidal-based model (Penasa et al., accepted) present in the panels above.

Once defined the regions of interest we verified the spectral separability of the ROIs, meaning that we controlled that they had a good class divergence. This was possible through two methods working in parallel, namely the Jeffries-Matusita and the Transformed Divergence (Richards & Jia,

2006) that indicate how well the selected ROIs pairs are statistically separate (Fig. 44).

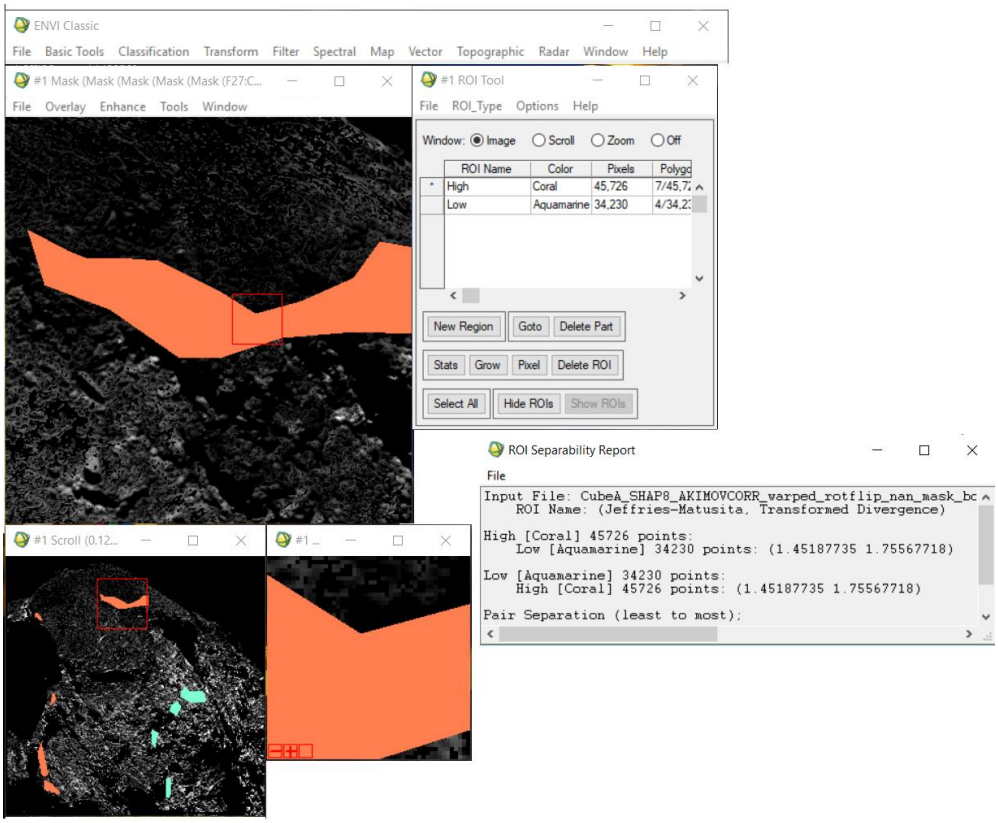

Fig. 44 ROIs separability computed using the Jeffries-Matusita and Transformed Divergence methods.

With the n-D visualizer tool we compared the reflectance distribution of the pixels assigned to each ROI between two (2D) or three (3D) bands: in both cases it was possible to notice that the classes, comparing all the bands, were not well separated and that generally the cluster representative of the outer shell had smaller reflectance values with respect to the inner shell.

Therefore we decided to intervene creating new classes and reducing the number of pixels for each ROI, using only the ones that mainly diverge from the other class: we decided thus to select pixel with lower reflectance for the outer outcrop and pixel with higher reflectance to identify the inner outcrop (Fig. 45 and Fig. 46).

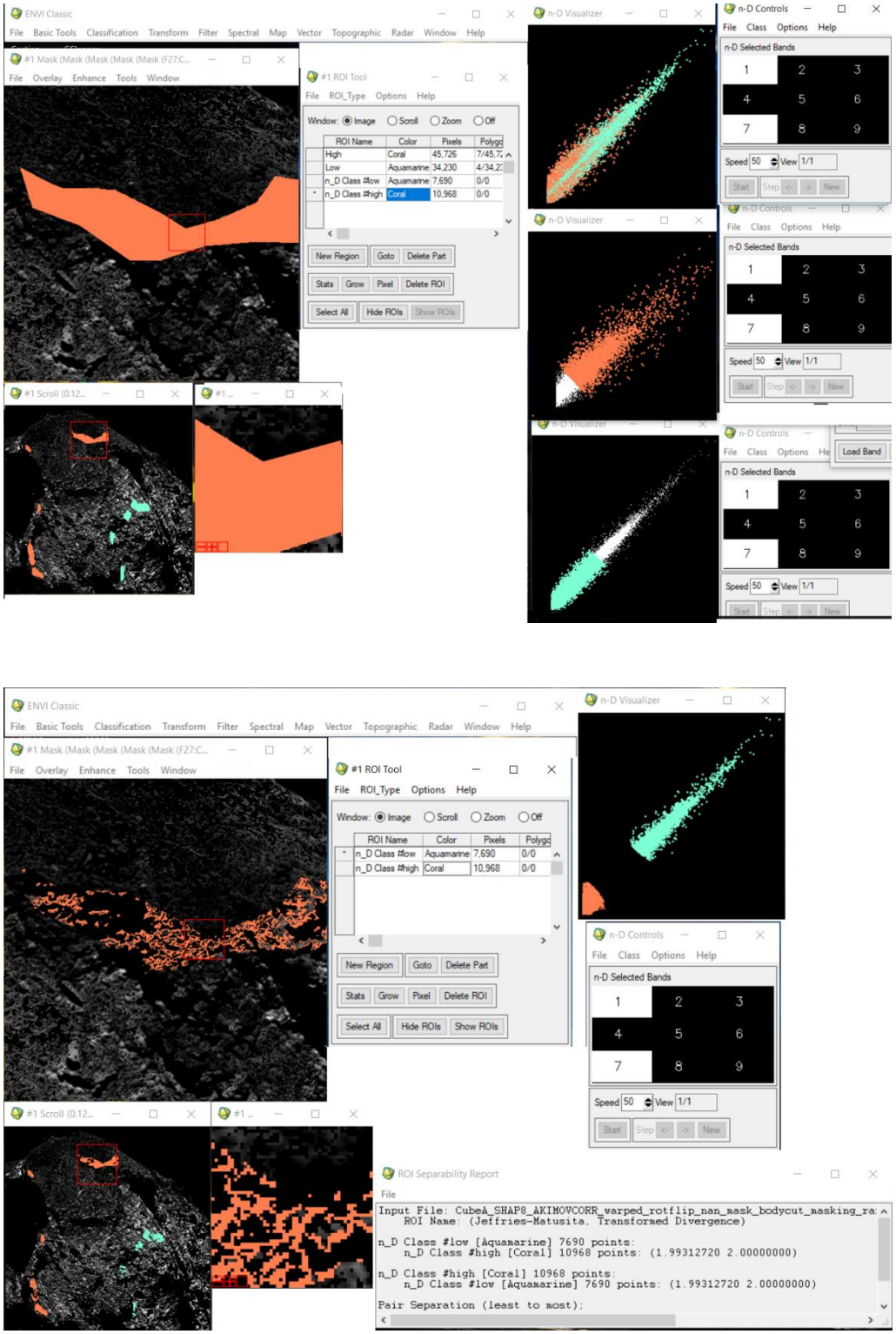

Fig. 45 ROIs reflectance distribution computed using Exelis Envi Classic n-D visualizer in ROI tool and successive creation of new ROIs (*on the panel above*) and new ROIs separability (*on the panel below*).

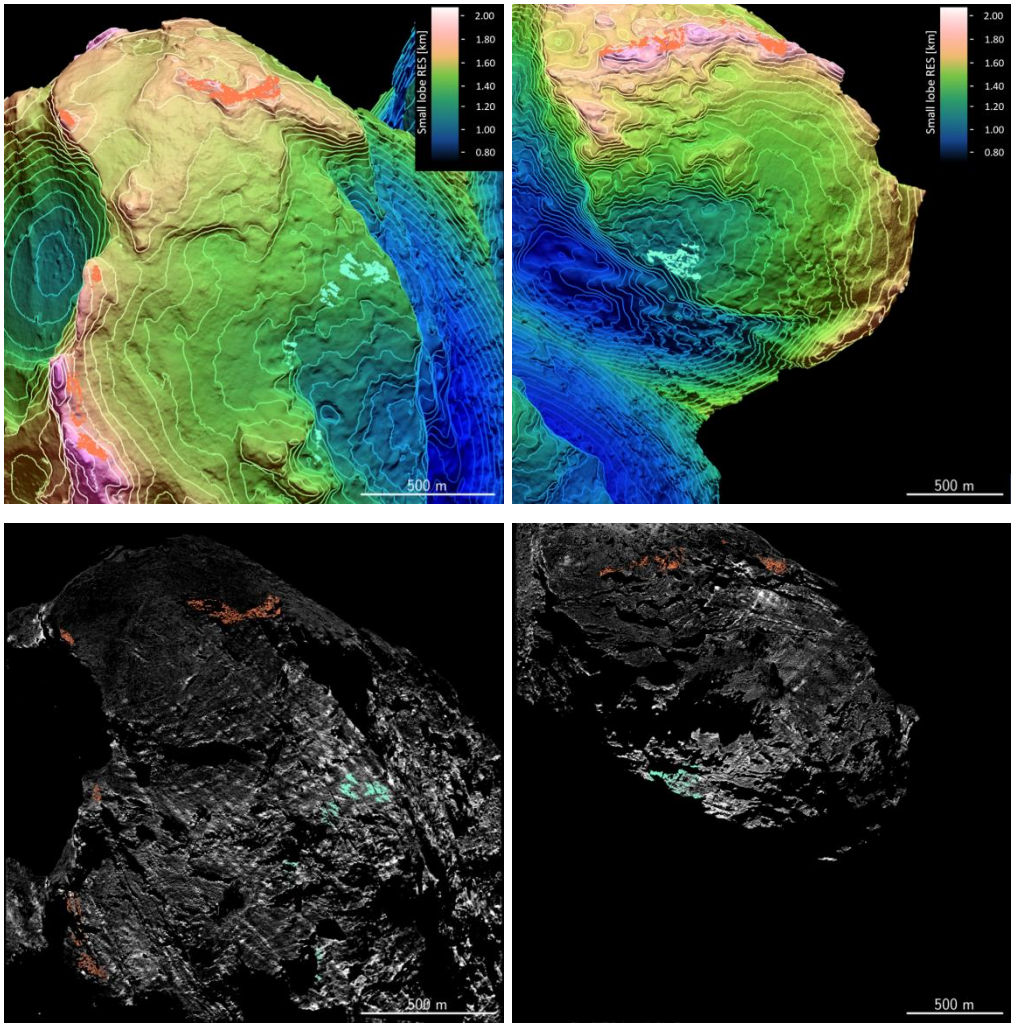

Fig. 46 New separate ROIs on cube A (*panels on the left*) and AB (*panels on the right*) with high and low elevations respectively in coral and aquamarine, also reported on the ellipsoidal-based model (Penasa et al., accepted) in the panels above.

Successively we performed a new supervised classification MLL that allowed to distinguish at least two shells: an inner and outer ones. The comparison between the obtained classification and the elevation model indicated that an innermost and outermost shells can be well identified, respectively representative of the part of Wosret toward Neith and of Bastet and the part of Wosret toward Maftet (Fig. 47).

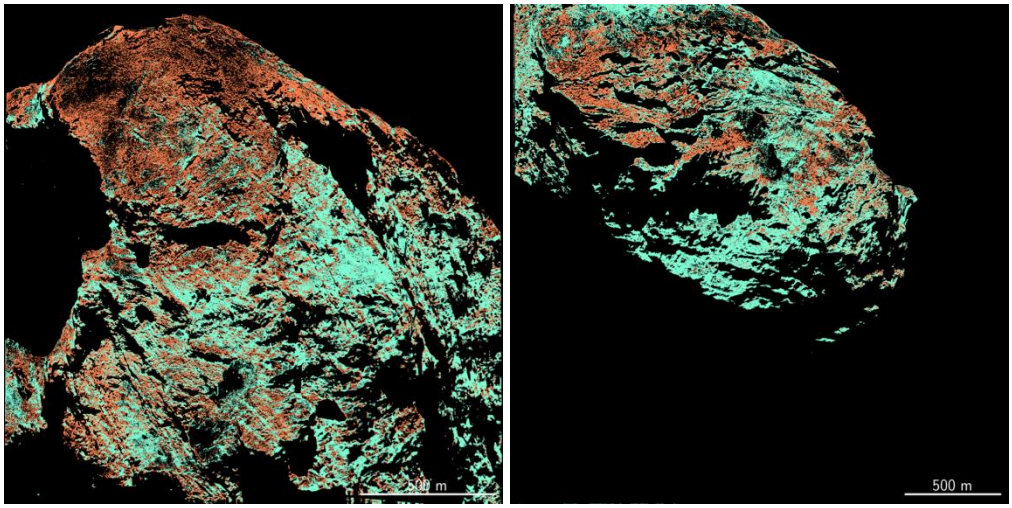

Fig. 47 Maximum Likelihood supervised classification on cube A (*on the left*) and AB (*on the right*) with an inner layer in aquamarine and an outer layer in coral.

Both for the inner and outer outcrop we extrapolated the spectral slope from the pixels attributed to each identified class, in order to compare the results between the two cubes (See ch. 5).

5. Results

In general, we observed that in both the cubes the outcrops pertaining to the innermost shells presented higher reflectance and spectral slopes with respect to the outermost ones. The same results were obtained both for cube A and AB (Fig. 48).

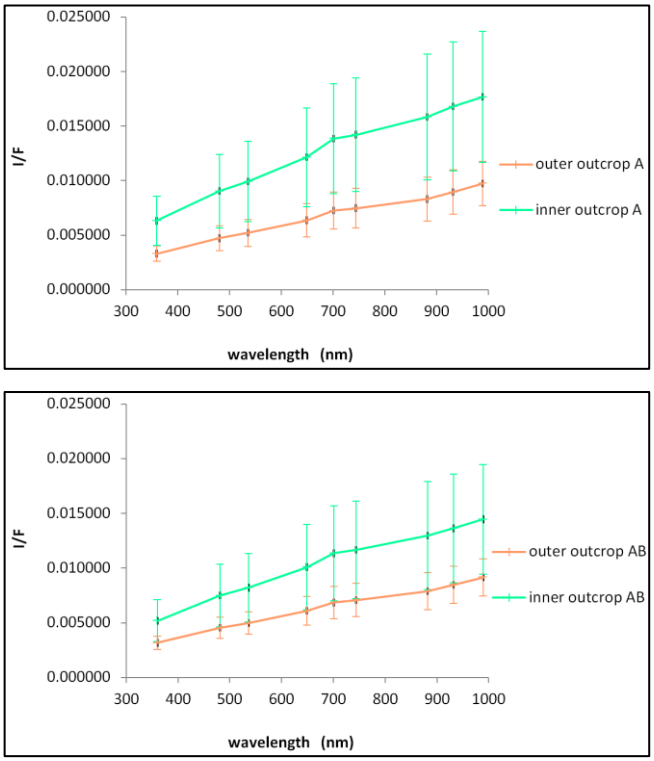

Fig. 48 Average spectra of inner (aquamarine color) and outer (coral color) outcrops for cube A (*above*) and AB (*below*) with the standard deviation bars.

Despite selected images were acquired five months after the perihelion passage, when the sublimation processes due to the cometary activity were notably reduced, the absolute spectral slopes of the classes on both cubes display an enhancement of the flux in the 700-750 nm range, probably associated with coma emissions (Fornasier et al., 2015).

We then normalized spectra to the green wavelength, centered on 536 nm, to be consistent with most of the literature data on primitive Solar System bodies, and obtained that all the spectra appear to have equal straight line slope with the exception of the portion of wavelength larger than 900 nm, where the

slope decreased at the transition between outermost and innermost layers (Fig. 49).

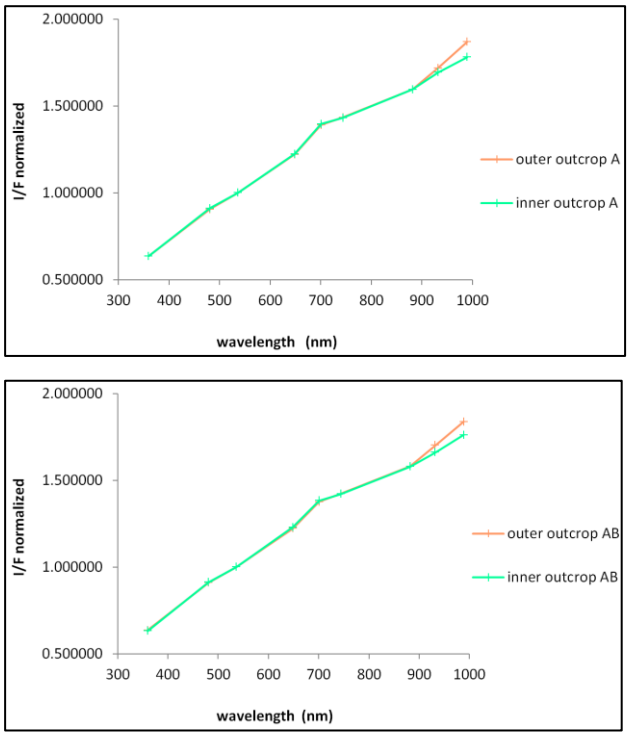

Fig. 49 Normalized spectra on 536 nm of the inner (aquamarine color) and outer (coral color) outcrops for cube A (*above*) and AB (*below*).

Comparing the values pertaining to the innermost shells to those of the outermost shells and confronting the results obtained for both cubes we observed that the main discriminant is the absolute reflectance rather than the spectral slope. This looked like a compositional variation between the shells even if too faint and possibly masked by the presence of fine material coatings.

Although the small dust coatings present in the lobe's southern hemisphere were removed from the classification, we decided to extrapolate the average spectra of the fine material, in order to obtain a reliable comparison between outcrops and fine materials. Instead of using the dust deposits present in our regions, which could be optically affected by the presence of the underlying outcrop, because of their extremely thin coating, we used the fine materials that fill the Hatmehit depression (northern hemisphere), which appear thick enough to be representative of this unit. For both cubes, the reflectance appeared similar to that of the innermost shells in the absolute spectra. Once

normalized, the fine material spectra display a slightly higher slope for wavelength longer than 700 nm with respect to the outcrops. Being normalized outcrops spectra nearly identical, no preferential similarity results between fine materials and one of the two shells (Fig. 50).

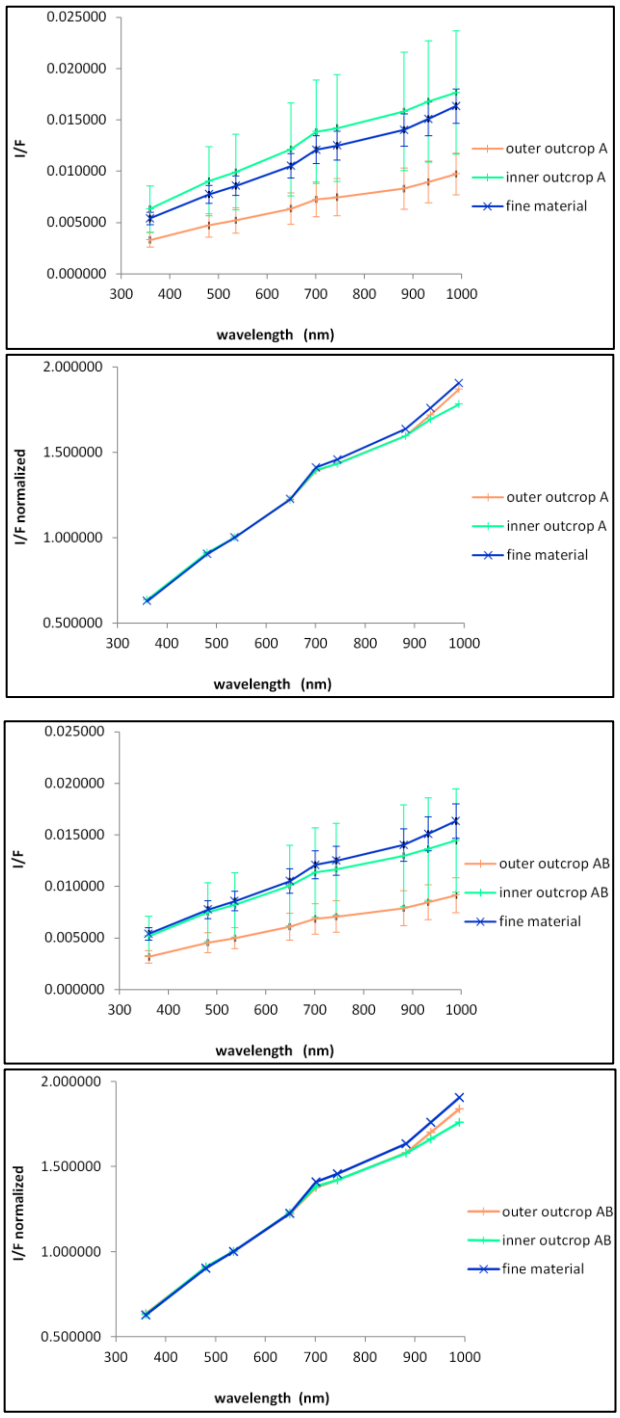

Fig. 50 Average spectra with standard deviation bars and normalized spectra on 536 nm of inner (aquamarine color) and outer (coral color) outcrops along with the fine material class (blue color) for cube A (*upper panels*) and AB (*bottom panels*).

We also performed a ratio between the inner and outer outcrop to verify the presence or absence of a constant multiplication factor in the various filters. A constant reflectance difference is indeed present for all filters of wavelength shorter than 900 nm, with cube AB more illuminated with respect to the other one (Fig. 51). The difference was probably due to an imperfect photometric correction.

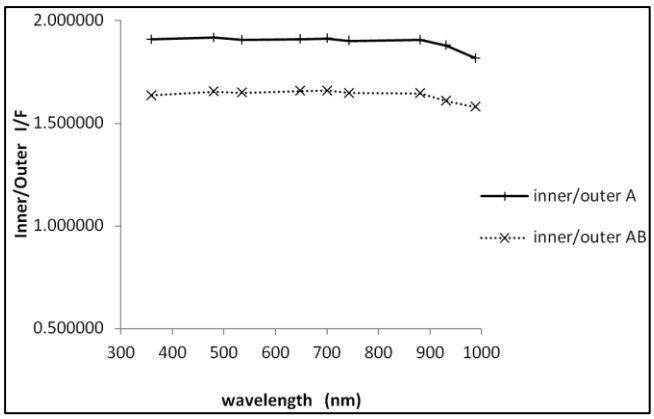

Fig. 51 Inner/Outer outcrop ratio.

Finally, we extrapolated the number of pixels occurring at each structural elevation, relatively to the elevation model (Penasa et al., accepted), obtaining for both the cubes an histogram related to each shell (i.e. inner and outer) (Fig. 52 and Fig. 53). Overall, the outer outcrops show a peak around 1.6-1.7 km of structural elevation, while the inner outcrops show a broader distribution inward with a peak around 1.4-1.5 km.

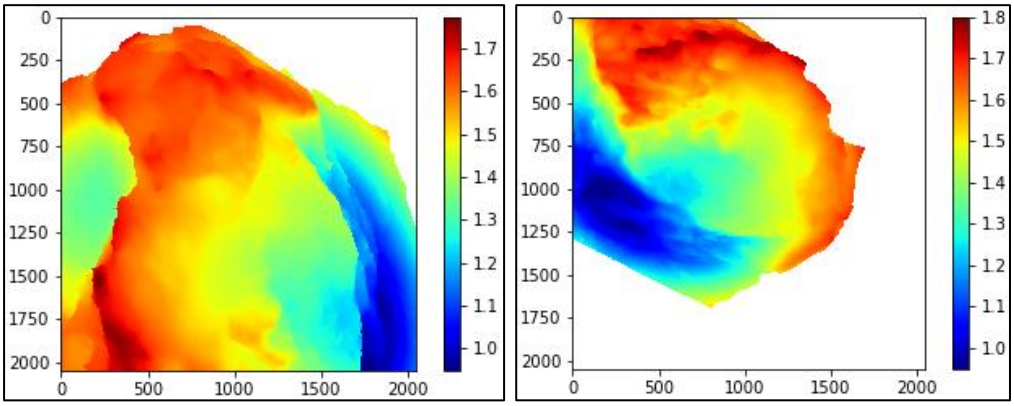

Fig. 52 Elevation models for cube A (*on the left*) and AB (*on the right*).

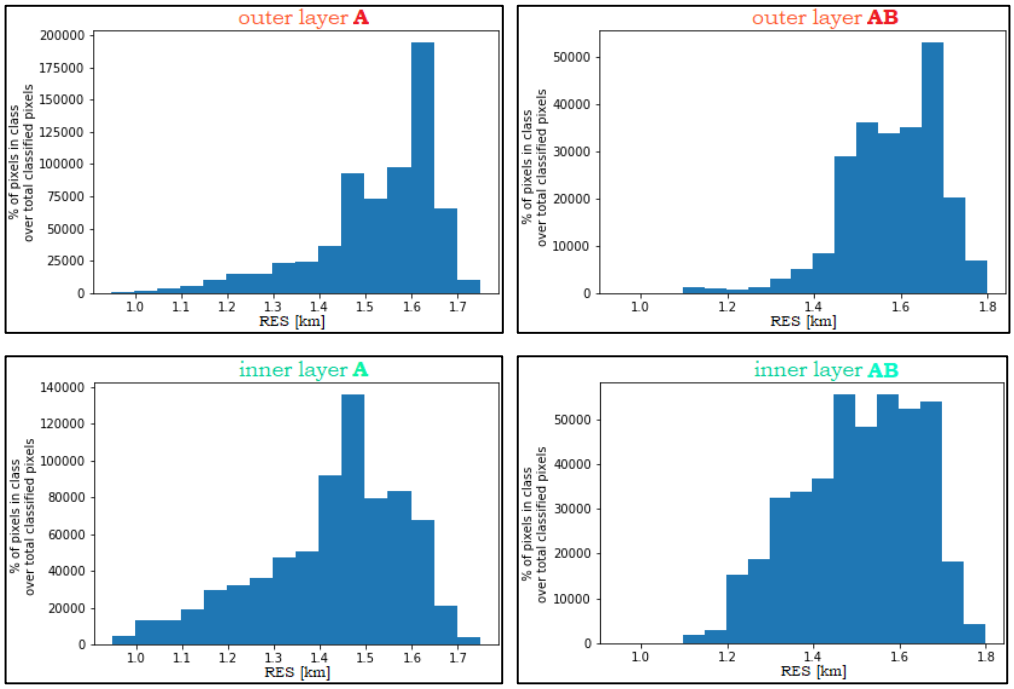

Fig. 53 Number of pixels occurring at each structural elevation relatively to the outer (*upper panels*) and inner (*bottom panels*) layers both for cube A (*on the left*) and AB (*on the right*).

Then we plotted the percentage of layer occupied by each class in function of the structural elevation and we verified that, in both cubes, increasing the distance from the center of the ellipsoid a class prevailed on the other (Fig. 54).

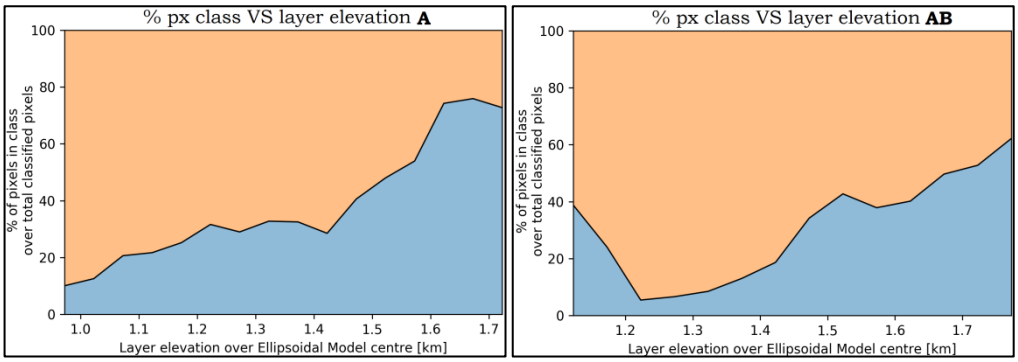

Fig. 54 Percentage of pixel pertaining to each class in function of the structural elevation both for cube A (*on the left*) and AB (*on the right*).

6. Conclusions

Our image classification highlighted a difference in absolute reflectance between the two proposed classes, showing higher values for the innermost shell and lower values for the outermost one (Fig. 55).

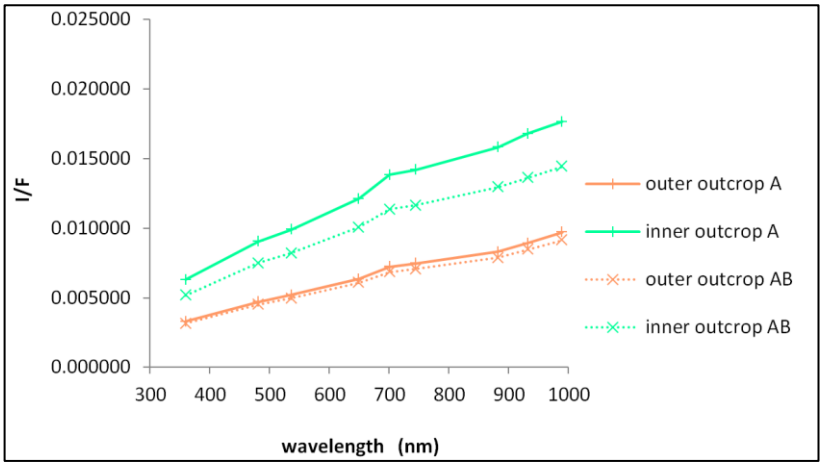

Fig. 55 Reassuming average spectra of outer and inner outcrops of cube A and AB.

A possible cause of the different reflectance between inner and outer layers could be potentially attributed to the different exposure of the outcrops to the space weathering, which could have altered their spectral appearance. In fact the bombardment by interplanetary dust particles and the irradiation by cosmic and solar wind ions, increased in particular during the perihelion approach, can induce relevant surface modifications on airless bodies, such as alteration processes that affect the spectral properties of silicate and icy materials leading to a darkening and reddening of the reflectance spectra (Brunetto et al., 2007). However, the exposition to the space weathering of the outer and inner layers are equivalent, preventing any discrimination on the basis of the space weathering degree. This suggests that the different level of brightness is more related to the compositional and/or textural properties of the outcropping layers in function of their diverse structural elevation in the ellipsoidal model (Penasa et al., accepted) rather than their degradation state. Indeed the consolidated materials present in Wosret toward the neck region,

show a higher reflectance and a lower structural elevation with respect to the ones present toward the Maftet region, which are characterized by a lower reflectance and a higher structural elevation (Fig. 56).

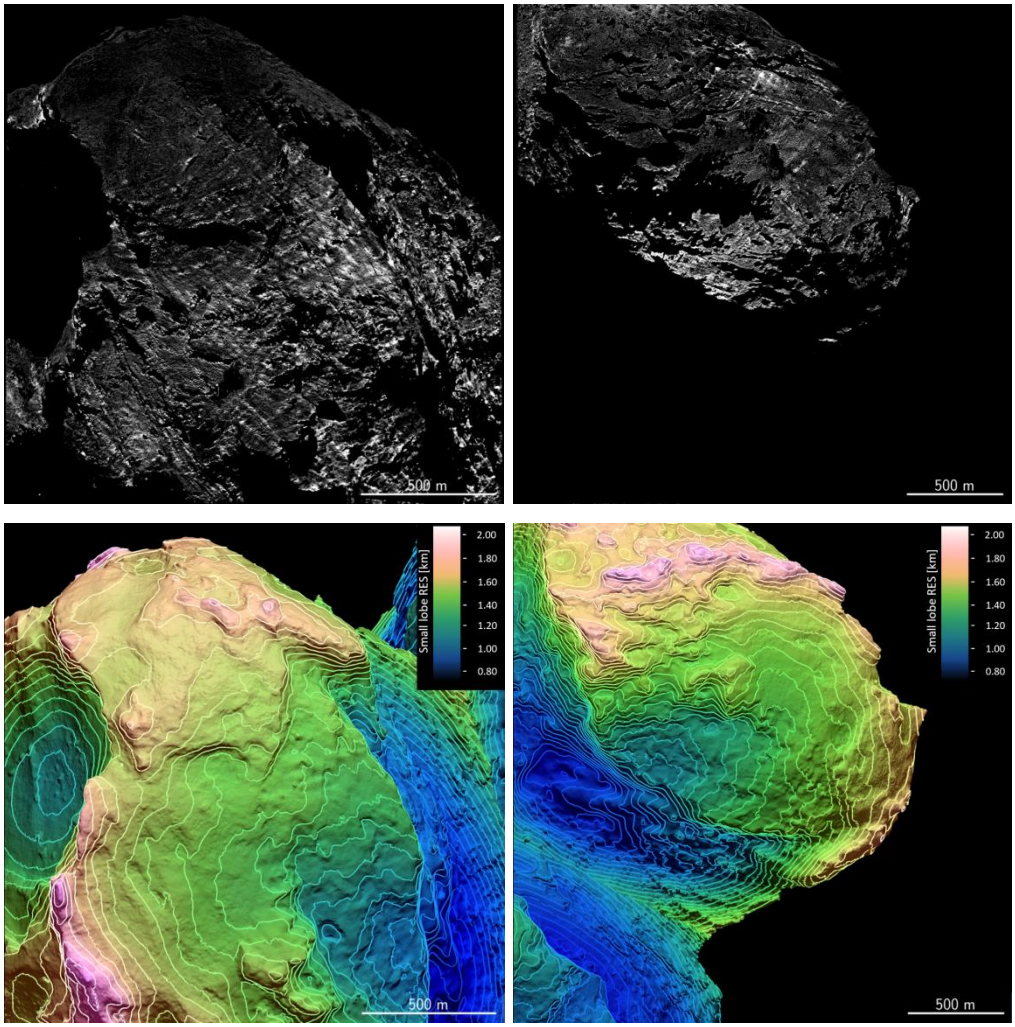

Fig. 56 Comparison between reflectance (*upper panels*) and structural elevation (*bottom panels*) of cube A (*on the left*) and AB (*on the right*).

The lack of significant differences in the normalized spectra prevents further considerations about the composition. On the other hand, assuming a homogeneous composition, the spectral variegation could be due to different textures of the nucleus surface.

Our results are comparable with the ones obtained for the bigger lobe of comet 67P (Ferrari et al., 2017), on Imhotep, Bes, Atum, Apis, Ash and Khonsu regions. These areas were investigated using post-perihelion

multispectral images acquired by the Narrow Angle Camera OSIRIS processed applying the same methodologies. Ferrari et al. (2017) performed the Maximum Likelihood supervised classification on consolidated outcrops and their relative deposits, allowing to identify two classes of consolidated cometary material located at different structural elevations and characterized by different brightness, with the innermost class brighter than the outermost one. This confirms that, even if once separated (Massironi et al., 2015), the two lobes had a qualitatively similar evolutionary histories before their merging.

Therefore we can conclude that the classification, applied on the two multispectral cubes obtained by the stacking and photometric correction of the two sets of post-perihelion images acquired by the OSIRIS NAC, led to the distinction of two classes of outcrops, with different structural level, with respect to the ellipsoidal-based model (Penasa et al., accepted), and different optical properties, with the inner class being brighter and localized on the innermost layers of our area and the outer class being darker and localized on the outermost layers. The photometric variegation observed between the innermost and outermost layers is thus mainly due to the surface brightness and could be attributed to different textures of the material constituting the cometary nucleus of 67P/Churyumov-Gerasimenko.

Bibliography

Akimov L.A., *Influence of mesorelief on the brightness distribution over a planetary disk*, Soviet Astronomy, 1976

Akimov L.A., *Light reflection by the Moon. I.*, Kinematika I Fizika Nebesnykh, 1988

Altwegg et al., *67P/Churyumov-Gerasimenko, a Jupiter family comet with a high D/H ratio*, Science, 2014

Asadi et al., *Mineralogy and formation conditions of Olivines, Pyroxenes and Carbonates in composition of Comets Nuclei*, Conference Paper, 2015

Brownlee D.E., *Comets*, in Meteorites, Comets and Planets, edited by Davis A.M., 2005

Brunetto, Orofino & Strazzulla, *Space weathering: from laboratory to observations*, Memorie della Società Astronomica Italiana Supplementi, 2007

Capaccioni et al., *The organic-rich surface of comet 67P/Churyumov-Gerasimenko as seen by VIRTIS/Rosetta*, Science, 2015

Ciarletti et al., *CONSERT suggests a change in local properties of 67P/Churyumov-Gerasimenko's nucleus at depth*, Astronomy & Astrophysics, 2015

Davidsson et al., *The primordial nucleus of 67P/Churyumov-Gerasimenko*, Astronomy & Astrophysics, 2016

De Sanctis et al., *The diurnal cycle of water ice on comet 67P/Churyumov-Gerasimenko*, Nature, 2015

Delsemme A.H., *Galactic tides affect the Oort Cloud: an observational confirmation*, Astronomy & Astrophysics, 1987

El-Maarry et al., *Regional surface morphology of comet 67P/Churyumov-Gerasimenko from Rosetta/OSIRIS images*, Astronomy & Astrophysics, 2015

El-Maarry et al., *Regional surface morphology of comet 67P/Churyumov-Gerasimenko from Rosetta/OSIRIS images: The southern hemisphere*, Astronomy & Astrophysics, 2016

Ernst & Schultz, *Evolution of the Deep Impact flash: implications for the nucleus surface based on laboratory experiments*, Icarus, 2007

Fernández J.A., *The formation of the Oort Cloud and the primitive galactic environment*, Icarus, 1997

Ferrari et al., *Comparison between layers stacks of 67P/CG comet and spectrophotometric variability obtained from OSIRIS data*, European Planetary Science Congress, 2017

Filacchione et al., *Compositional maps of 67P/CG nucleus by ROSETTA/VIRTIS-M*, 46th Lunar and Planetary Science Conference, 2015

Fornasier et al., *Spectrophotometric properties of the nucleus of comet 67P/Churyumov-Gerasimenko from OSIRIS instrument onboard the ROSETTA spacecraft*, Astronomy & Astrophysics, 2015

Fornasier et al., *Rosetta's comet 67P/Churyumov-Gerasimenko sheds its dusty mantle to reveal its icy nature*, Science, 2016

Fulle et al., *Unexpected and significant findings in comet 67P/Churyumov-Gerasimenko: an interdisciplinary view*, Monthly Notices of the Royal Astronomical Society, 2016

Keller et al., *OSIRIS – The scientific camera system onboard Rosetta*, Space Science Reviews, 2007

Keller et al., *E-type Asteroid (2867) Steins as imaged by OSIRIS on board Rosetta*, Science, 2010

Kofman et al., *Properties of the 67P/Churyumov-Gerasimenko interior revealed by CONSERT radar*, Science, 2015

La Forgia et al., *Geomorphology and spectrophotometry of Philae's landing site on comet 67P/Churyumov-Gerasimenko*, Astronomy & Astrophysics, 2015

Lamy et al., *A portrait of the nucleus of comet 67P/Churyumov-Gerasimenko*, Space Science Reviews, 2007

Lee et al., *Geomorphological mapping of comet 67P/Churyumov-Gerasimenko's southern hemisphere*, Monthly Notices of the Royal Astronomical Society, 2016

Levison H.F., *Comet taxonomy*, Completing the Inventory of the Solar System, 1996

Lyttleton R.A., *On the origin of comets*, Monthly Notices of the Royal Astronomical Society, 1948

Massironi et al., *Two independent and primitive envelopes of the bilobate nucleus of comet 67P*, Nature, 2015

Morbidelli & Rickman, *Comets as collisional fragments of a primordial planetesimal disk*, Astronomy & Astrophysics, 2015

Oort J.H., *The structure of the cloud of comets surrounding the Solar System, and a hypothesis concerning its origin*, Bulletin of the Astronomical Institutes of the Netherlands, 1950

Pätzold et al., *A homogeneous nucleus for comet 67P/Churyumov-Gerasimenko from its gravity field*, Nature, 2016

Penasa et al., *A three dimensional modeling of the layered structure of comet 67P/Churyumov-Gerasimenko*, MNRAS, accepted

Preusker et al., *Shape model, reference system definition, and cartographic mapping standards for comet 67P/Churyumov-Gerasimenko – Stereo-photogrammetric analysis of Rosetta/OSIRIS image data*, Astronomy & Astrophysics, 2015

Richards & Jia, *Remote sensing digital image analysis*, Remote sensing digital image analysis, 2006

Shkuratov et al., *Principle of undulatory invariance in photometry of atmosphereless celestial bodies*, Icarus, 1994

Shkuratov et al., *Classical photometry of prefractal surfaces*, Optical Society of America Journal, 2003

Shkuratov et al., *Optical measurements of the Moon as a tool to study its surface*, Planetary and Space Science, 2011

Sierks et al., *Images of Asteroid 21 Lutetia: a remnant planetesimal from the early Solar System*, Science, 2011

Sierks et al., *On the nucleus structure and activity of comet 67P/Churyumov-Gerasimenko*, Science, 2015

Thomas et al., *The morphological diversity of comet 67P/Churyumov-Gerasimenko*, Science, 2015

Vincent et al., *Large heterogeneities in comet 67P as revealed by active pits from sinkhole collapse*, Nature, 2015

Weissman et al., *Structure and density of cometary nuclei*, Comets II 2004

Whipple F.L., *A comet model. I. The acceleration of Comet Encke*, Astrophysical Journal, 1950

Wiegert & Tremaine, *The evolution of long-period comets*, Icarus, 1998

Acknowledgments

I would like to express the deepest appreciation to my supervisor, Prof. Matteo Massironi, who introduced me to the planetary geology and made it possible for me to work on a topic that is of great interest to me. It was a pleasure working with him.

I thank profusely Dr.Sabrina Ferrari and Dr. Fiorangela La Forgia for their kind help and co-operation throughout my research period. They never stopped challenging me, helping me develop my ideas and showing confidence in my work.

In addition, a thank to Dr. Luca Penasa who participated in this research with interest and enthusiasm.

Finally, I would like to acknowledge with gratitude the support and love of my family and friends, who supported me during all my academic career.